
VOLUME 332 ISSUE 23
11 NOVEMBER 2013
ISSN 0022-460X
ELSEVIER
JOURNAL OF SOUND AND VIBRATION
Available online at www.sciencedirect.com
ScienceDirect

Journal of Sound and Vibration 332 (2013) 6128–6154

Contents lists available at ScienceDirect

Journal of Sound and Vibration

journal homepage: www.elsevier.com/locate/jsvi

Nonlinear dynamic analysis of a rotor-bearing-seal system under two loading conditions

Hui Ma *, Hui Li, Heqiang Niu, Rongze Song, Bangchun Wen

School of Mechanical Engineering and Automation, Northeastern University, Shenyang, Liaoning 110819, PR China

A R T I C L E I N F O

Article history:
Received 13 December 2012
Received in revised form
18 April 2013
Accepted 14 May 2013
Handling Editor: J. Lam
Available online 20 July 2013

A B S T R A C T

The operating speed of the rotating machinery often exceeds the second or even higher order critical speeds to pursue higher efficiency. Thus, how to restrain the higher order mode instability caused by the nonlinear oil-film force and seal force at high speed as far as possible has become more and more important. In this study, a lumped mass model of a rotor-bearing-seal system considering the gyroscopic effect is established. The graphite self-lubricating bearing and the sliding bearing are simulated by a spring-damping model and a nonlinear oil-film force model based on the assumption of short bearings, respectively. The seal is simulated by Muszynska nonlinear seal force model. Effects of the seal force and oil-film force on the first and second mode instabilities are investigated under two loading conditions which are determined by API Standard 617 (Axial and Centrifugal Compressors and Expander-compressors for Petroleum, Chemical and Gas Industry Services, Seventh Edition). The research focuses on the effects of exciting force forms and their magnitudes on the first and second mode whips in a rotor-bearing-seal system by using the spectrum cascades, vibration waveforms, orbits and Poincaré maps. The first and second mode instability laws are compared by including and excluding the seal effect in a rotor system with single-diameter shaft and two same discs. Meanwhile, the instability laws are also verified in a rotor system with multi-diameter shaft and two different discs. The results show that the second loading condition (out-of-phase unbalances of two discs) and the nonlinear seal force can mainly restrain the first mode instability and have slight effects on the second mode instability. This study may contribute to a further understanding about the higher order mode instability of such a rotor system with fluid-induced forces from the oil-film bearings and seals.

1. Introduction

Modern rotating machines, such as turbines, compressors, generators, are designed for high speed, flexibility and efficiency. In order to avoid unstable vibrations at higher operating speeds, more and more attention has been paid on the self-excited vibration, which is induced by the interaction between the rotor and surrounding fluid. Fluid-induced forces mainly include the force from the oil-film bearings and seals. It can lead to significant alternating stresses in the rotor, the high-level vibration, the rubbing between the rotor and the stator and the potential damage of the rotating machinery eventually. So the research on the mechanism of fluid–solid interaction in the rotor-bearing-seal system is of great importance for modern rotating machines.

* Corresponding author. Tel./fax: +86 248 3684491.
E-mail address: mahui_2007@163.com (H. Ma).

0022-460X/$ - see front matter © 2013 Elsevier Ltd. All rights reserved.
http://dx.doi.org/10.1016/j.jsv.2013.05.014

Nomenclature

c	bearing clearance
c_{blx}, c_{bly}	dampings of the left bearing in x and y directions
c_f	radial clearance of seal
$\mathbf{C}$	damping matrix of the global system
$\mathbf{C}_1$	Rayleigh damping matrix
$\mathbf{C}_2$	bearing damping matrix
D	bearing diameter
D_f	equivalent damping
e_f	the radio of the rotor radial displacement to seal clearance
E	Young's modulus of elasticity
f_r	rotating frequency
f_{bx5}, f_{by5}	dimensionless oil-film forces in x and y directions
f_{n1},f_{n2}	the first and second mode whirl/whip frequencies
$\mathbf{F}_b$	oil-film force vector of the bearing
F_{bx5}, F_{by5}	oil-film forces in x and y directions
$\mathbf{F}_e$	unbalanced force vector of the rotor system
$\mathbf{F}_s$	nonlinear seal force vector of the rotor system
F_{sx3}, F_{sx4}, F_{sy3},F_{sx4}	nonlinear seal forces of the disc 1 and disc 2 in x and y directions
g	acceleration of gravity
$\mathbf{G}$	gyroscopic matrix
I	moment of inertia
$J_{di}(i=1,2,3,4,5)$	diametral moment of inertia of lumped points
$J_{pi}(i=1,2,3,4,5)$	polar moment of inertia of lumped points
$\mathbf{K}$	stiffness matrix of the global system
K_f	equivalent stiffness
l_f	length of seal
l_i	the distance between every two consecutive lumped mass points
L	bearing length
m_f	equivalent mass
m_i $(i=1,2,3,4,5)$	lumped mass
m_3r, m_4r	unbalance moments of two discs
m_0, n_0	experiential coefficients, determined by experiments and material structure of seal
$\mathbf{M}$	general mass matrix of the global system
ΔP	pressure margin of seal
$\mathbf{q}$	displacement vector
$\tilde{\mathbf{q}}$	dimensionless displacement vector
r	eccentricity of the disc
R_f	radius of seal
v	axial fluid speed
x_i, y_i $(i=1,2,3,4,5)$	displacements in x and y directions
$\tilde{x}_i, \tilde{y}_i (i=1,2,3,4,5)$	dimensionless displacements in x and y directions
η	lubricant viscosity
θ_{xi}, θ_{yi}	angles of orientation associated with the x and y axes
ξ	inlet loss coefficient
ξ_1, ξ_2	the first and second modal damping ratios
τ_f	fluid average circumferential velocity ration
υ	fluid dynamic viscous coefficient
φ_1, φ_2	initial phase angle of two discs
ω	rotating speed of rotor
ω_{n1}, ω_{n2}	the first and second natural frequencies

In earlier studies, the linear stiffness and damping coefficients are widely adopted to simulate the dynamic characteristics of bearings and seals [1,2]. However, the observed phenomena show that the bearing and seal fluid forces present strong nonlinearity. And the linear model will fail to analyze the nonlinear dynamic behaviors of the rotor-bearing-seal system under some conditions, such as the large perturbed motion of the journal.

In order to simulate the nonlinearity of the sliding bearing better, some nonlinear oil-film force models have been proposed, such as in papers [3–5]. Based on Capone model, Adiletta et al. [6] analyzed the possible chaotic motions resulted from the nonlinear response of bearings; Jing et al. [7,8] studied the nonlinear dynamic behaviors of a rotor-bearing system considering the oil whip phenomenon; de Castro et al. [9] researched the system instability threshold influenced by the unbalance, rotor arrangement form and bearing parameters; Ding et al. [10] analyzed the non-stationary dynamic responses of the system during speed-up with a constant angular acceleration for a multi-bearing rotor. Based on the non-steady nonlinear oil-film force model presented by Zhang [5], Ding et al. [11] analyzed non-stationary processes of a rotor-bearing system by taking the rotating angular speed as control parameter. In his another paper [12], Ding et al. studied dimension reductions of a continuous rotor system by the standard Galerkin method and the nonlinear Galerkin method, and his results revealed that transitions or bifurcations of the rotor whirl from being synchronous to nonsynchronous as the unstable speed was exceeded. Zhang et al. [13] presented a mathematical model and a computational methodology to simulate the complicated flow behaviors of the journal microbearing in the slip regime, and their investigation showed that the rotor motion was stable with half-frequency whirling when the system located in the lower stability region, and the rotor had high-frequency whirling when the system located in the upper stability region.

The seal force models have also been developed by many researchers. Alford [14] derived the formula of the gas exciting force first to research on the stability of aeroengine. The Alford model could explain some basic phenomena, but it was a simple linear one. Based on Hirs' turbulent lubrication equations, Childs [15] derived dynamic coefficient expressions for high-pressure annular seals typical of neck-ring and interstage seals employed in multistage centrifugal pumps. Muszynska [16,17] proposed a simple model of nonlinear fluid dynamic force generated in the seal based on the results of a series of experiments.

Based on Muszynska nonlinear seal force model, Li et al. [18] determined the empirical parameters of gas exciting force of the Muszynska model by using the results of computational fluid dynamics (CFD); Li et al. [19] analyzed dynamic behaviors of an unbalanced rotor-seal system with sliding bearings based on Floquet theory and the bifurcation theorem; Hua et al. [20] established a nonlinear model of rotor-seal system and investigated the nonlinear behavior of the unbalanced rotor-seal system by using an efficient and high-precision direct integration method; Ding et al. [21] investigated a symmetric rotor/seal system and analyzed the Hopf bifurcation of the system; Wang et al. [22] established a nonlinear mathematical model for orbital motion of the rotor system under the influence of leakage flow through an interlocking seal.

Considering the coupled effect of the nonlinear oil-film force and seal force, many researchers studied the dynamic behaviors of the rotor-bearing-seal system. Cheng et al. [23,24] and Shen et al. [25,26] investigated nonlinear dynamic behaviors of a rotor-bearing-seal coupled system by using the nonlinear oil-film forces obtained under the short bearing theory and Muszynska nonlinear seal force model. Based on an unsteady oil-film force proposed by Zhang and Muszynska seal force model, Li et al. [27,28] established a new dynamic model of a rotor system by the Hamilton principle and the finite element method, and they analyzed the coupled effects of the nonlinear oil-film force, the nonlinear seal force, and the mass eccentricity of the disc; Wang et al. [29] studied the nonlinear coupling vibrations excited by a labyrinth seal and two air-film journal bearings through numerical simulations for high-speed centrifugal compressors.

It should be noted that in all the above researches, only the first mode instability (oil whirl/whip) was concerned. In fact, the operating speed of the rotating machinery often exceeds the second or even higher order critical speed to pursue higher efficiency. Thus, the second mode instability can appear when the operating speed approaches or exceeds twice the second-order critical speed according to the literatures [16,30-32]. The researches about the coupled effects of the nonlinear oil-film force and seal force on the second mode instability have not been found. In this paper, influences of the nonlinear oil-film force coupled with seal force on the first and the second mode instabilities of a rotor-bearing-seal system, attached with two discs, are investigated. A nonlinear oil-film force model under short bearing assumption [3,4] and Muszynska seal force model [16,17] are adopted. Numerical integrations are used to get the solutions because of the nonlinearity of oil-film and seal forces. Spectrum cascade, vibration waveform, orbit and Poincaré map are applied to analyze various nonlinear phenomena and system unstable processes.

This paper consists of five sections. After this introduction, in Section 2, mathematical model of a rotor-bearing-seal system is established considering the nonlinearity of sliding bearing and seal. In Section 3, the first and second mode instability laws are compared by including and excluding the seal effect in a rotor system with single-diameter shaft and two same discs (simulation 1), and the effects of rotating speeds and eccentricities of disc on system instability are discussed under two loading conditions. Then, for examining the universality of simulation 1, Section 4 analyzes the instability laws in a rotor system with multi-diameter shaft and two different discs (simulation 2) under two loading conditions by adopting the same analysis method as that in Section 3. Finally, some conclusions are drawn in Section 5.

2. Mathematical model of a rotor-bearing-seal system with two discs

In order to study oil-film instability efficiently, a mathematical model of a rotor-bearing-seal system, which is depicted in Fig. 1, is simplified according to the following assumptions:

(a) The movements of the rotor in torsional and axial directions are negligible; the journals, coupling and discs are simulated by five lumped mass points and the corresponding points are connected by massless shaft sections of lateral stiffness; each point has four degrees of freedom including two rotations and two translations, as is shown in Fig. 1b. In the figure, m_i ($i=1,2,3,4,5$) and ω are lumped masses and rotating speed respectively.
(b) The left bearing shown in Fig. 1b is a graphite bearing, which is simulated by a spring-damping model in this paper, and the right one is a sliding bearing simulated by a nonlinear oil-film force model [3,4].

2.1. Equation of motion

The dynamic equation of the rotor-bearing-seal system with twenty degrees of freedom can be deduced as follows:

$$\mathbf{M}\ddot{\mathbf{q}} + (\mathbf{G}+\mathbf{C})\dot{\mathbf{q}} + \mathbf{K}\mathbf{q} = \mathbf{F}_e + \mathbf{F}_b + \mathbf{F}_s - \mathbf{F}_g, \tag{1}$$

$$\mathbf{q} = [x_1, \theta_{y1}, x_2, \theta_{y2}, x_3, \theta_{y3}, x_4, \theta_{y4}, x_5, \theta_{y5}, y_1, \theta_{x1}, y_2, \theta_{x2}, y_3, \theta_{x3}, y_4, \theta_{x4}, y_5, \theta_{x5}]^{\mathrm{T}} \tag{2}$$

where x_i, y_i, θ_{xi} and θ_{yi} ($i=1,2,3,4,5$) are the displacements in x and y directions and angles of orientation associated with the x and y axes, respectively.

$$\mathbf{M} = \begin{bmatrix} \mathbf{M}_x & \mathbf{0} \\ \mathbf{0} & \mathbf{M}_y \end{bmatrix}, \quad \mathbf{M}_x = \mathbf{M}_y = \mathrm{diag}[m_1, J_{d1}, m_2, J_{d2}, m_3, J_{d3}, m_4, J_{d4}, m_5, J_{d5}] \tag{3}$$

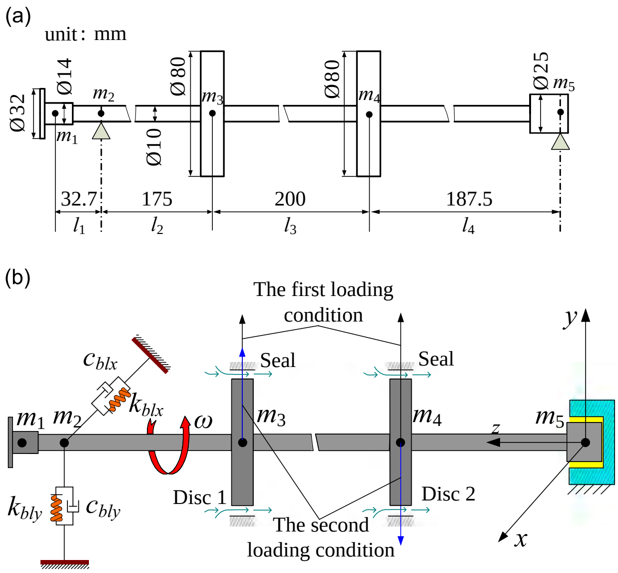

Fig. 1. Physical dimension and schematic diagram of a rotor-bearing-seal system: (a) physical dimension and (b) schematic diagram.

$$\mathbf{G}=\omega\mathbf{J}=\omega\begin{bmatrix}\mathbf{0} & \mathbf{J}_1\\ -\mathbf{J}_1^{\mathrm{T}} & \mathbf{0}\end{bmatrix},\quad \mathbf{J}_1=\mathrm{diag}[0,J_{p1},0,J_{p2},0,J_{p3},0,J_{p4},0,J_{p5}], \tag{4}$$

where J_{pi} and J_{di} $(i=1,2\ldots5)$ are the polar moment of inertia and the diametral moment of inertia of lumped mass points, respectively.

$$\mathbf{K}=\begin{bmatrix}\mathbf{K}_x & \mathbf{0}\\ \mathbf{0} & \mathbf{K}_y\end{bmatrix}, \tag{5}$$

$$\mathbf{K}_x=\begin{bmatrix}
k_{11} & k_{12} & k_{13} & k_{14} & 0 & 0 & 0 & 0 & 0 & 0\\
k_{12} & k_{22} & k_{23} & k_{24} & 0 & 0 & 0 & 0 & 0 & 0\\
k_{13} & k_{23} & k_{33}+k_{blx} & k_{34} & k_{35} & k_{36} & 0 & 0 & 0 & 0\\
k_{14} & k_{24} & k_{34} & k_{44} & k_{45} & k_{46} & 0 & 0 & 0 & 0\\
0 & 0 & k_{35} & k_{45} & k_{55} & k_{56} & k_{57} & k_{58} & 0 & 0\\
0 & 0 & k_{36} & k_{46} & k_{56} & k_{66} & k_{67} & k_{68} & 0 & 0\\
0 & 0 & 0 & 0 & k_{57} & k_{67} & k_{77} & k_{78} & k_{79} & k_{7,10}\\
0 & 0 & 0 & 0 & k_{58} & k_{68} & k_{78} & k_{88} & k_{89} & k_{8,10}\\
0 & 0 & 0 & 0 & 0 & 0 & k_{79} & k_{89} & k_{99} & k_{9,10}\\
0 & 0 & 0 & 0 & 0 & 0 & k_{7,10} & k_{8,10} & k_{9,10} & k_{10,10}
\end{bmatrix} \tag{6}$$

$$\mathbf{K}_y=\begin{bmatrix}
k_{11} & -k_{12} & k_{13} & -k_{14} & 0 & 0 & 0 & 0 & 0 & 0\\
-k_{12} & k_{22} & -k_{23} & k_{24} & 0 & 0 & 0 & 0 & 0 & 0\\
k_{13} & -k_{23} & k_{33}+k_{bly} & -k_{34} & k_{35} & -k_{36} & 0 & 0 & 0 & 0\\
-k_{14} & k_{24} & -k_{34} & k_{44} & -k_{45} & k_{46} & 0 & 0 & 0 & 0\\
0 & 0 & k_{35} & -k_{45} & k_{55} & -k_{56} & k_{57} & -k_{58} & 0 & 0\\
0 & 0 & -k_{36} & k_{46} & -k_{56} & k_{66} & -k_{67} & k_{68} & 0 & 0\\
0 & 0 & 0 & 0 & k_{57} & -k_{67} & k_{77} & -k_{78} & k_{79} & -k_{7,10}\\
0 & 0 & 0 & 0 & -k_{58} & k_{68} & -k_{78} & k_{88} & -k_{89} & k_{8,10}\\
0 & 0 & 0 & 0 & 0 & 0 & k_{79} & -k_{89} & k_{99} & -k_{9,10}\\
0 & 0 & 0 & 0 & 0 & 0 & -k_{7,10} & k_{8,10} & -k_{9,10} & k_{10,10}
\end{bmatrix} \tag{7}$$

The matrix elements of $\mathbf{K}_x$ and $\mathbf{K}_y$ are as follows:

$$\begin{cases} k_{11}=a_{11} \\ k_{12}=a_{21} \\ k_{13}=-a_{11} \\ k_{14}=a_{21} \end{cases}, \quad \begin{cases} k_{22}=l_1a_{21}-a_{31} \\ k_{23}=-a_{21} \\ k_{24}=a_{31} \end{cases}, \quad \begin{cases} k_{33}=a_{11}+a_{12} \\ k_{34}=-a_{21}+a_{22} \\ k_{35}=-a_{12} \\ k_{36}=a_{22} \end{cases},$$

$$\begin{cases} k_{44}=l_1a_{21}-a_{31}+l_2a_{22}-a_{32} \\ k_{45}=-a_{22} \\ k_{46}=a_{32} \end{cases}, \quad \begin{cases} k_{55}=a_{12}+a_{13} \\ k_{56}=-a_{22}+a_{23} \\ k_{57}=-a_{13} \\ k_{58}=a_{23} \end{cases}, \begin{cases} k_{66}=l_2a_{22}-a_{32}+l_3a_{23}-a_{33} \\ k_{67}=-a_{23} \\ k_{68}=a_{33} \end{cases},$$

$$\begin{cases} k_{77}=a_{13}+a_{14} \\ k_{78}=-a_{23}+a_{24} \\ k_{79}=-a_{14} \\ k_{7,10}=a_{24} \end{cases}, \quad \begin{cases} k_{88}=l_3a_{23}-a_{33}+l_4a_{24}-a_{34} \\ k_{89}=-a_{24} \\ k_{8,10}=a_{34} \end{cases}, \quad \begin{cases} k_{99}=a_{14} \\ k_{9,10}=-a_{24} \\ k_{10,10}=l_4a_{24}-a_{34} \end{cases},$$

where k_{blx} and k_{bly} denote the stiffnesses of the left bearing in x and y directions, respectively. And

$$\begin{cases} a_{1i}=\frac{12EI}{l_i^3} \\ a_{2i}=\frac{1}{2}l_ia_{1i}, \quad i=1,2,3,4, \\ a_{3i}=\frac{1}{6}l_i^2a_{1i} \end{cases} \tag{8}$$

in which E, l_i (i=1,2…4) and I are the Young's modulus of elasticity, the distance between every two consecutive lumped mass points and the area moment of inertia respectively.

$$\mathbf{C}=\mathbf{C}_1+\mathbf{C}_2, \tag{9}$$

$$\mathbf{C}_1=\alpha\mathbf{M}+\beta\mathbf{K}, \tag{10}$$

$$\alpha=\frac{60(\omega_{n2}\xi_1-\omega_{n1}\xi_2)\omega_{n1}\omega_{n2}}{\pi(\omega_{n2}^2-\omega_{n1}^2)}, \quad \beta=\frac{\pi(\omega_{n2}\xi_2-\omega_{n1}\xi_1)}{15(\omega_{n2}^2-\omega_{n1}^2)}, \tag{11}$$

where ω_{n1} and ω_{n2} are the first and second natural frequencies (rev/min); ξ_1 and ξ_2 are the first and second modal damping ratios, respectively.

$$\mathbf{C}_2=\mathrm{diag}[0,0,c_{blx},0,0,0,0,0,0,0,0,0,c_{bly},0,0,0,0,0,0,0], \tag{12}$$

in which c_{blx} and c_{bly} are the dampings of the left bearing in x and y directions respectively.

$$\begin{aligned}\mathbf{F}_e=[&0,0,0,0,m_3r\omega^2\cos(\omega t+\varphi_1),0,m_4r\omega^2\cos(\omega t+\varphi_2),0,0,0,\\ &0,0,0,0,m_3r\omega^2\sin(\omega t+\varphi_1),0,m_4r\omega^2\sin(\omega t+\varphi_2),0,0,0]^{\mathrm{T}}.\end{aligned} \tag{13}$$

Here m_3r, m_4r, φ_1 and φ_2 denote unbalance moments of the left and right discs, initial phase angles of eccentricity in left and right discs, respectively.

$$\mathbf{F}_b=[0,0,0,0,0,0,0,0,0,F_{bx5},0,0,0,0,0,0,0,0,0,F_{by5},0]^{\mathrm{T}} \tag{14}$$

where F_{bx5} and F_{by5} are nonlinear oil-film forces of the right bearing in x and y directions.

$$\mathbf{F}_g=[0,0,0,0,0,0,0,0,0,0,m_1g,0,m_2g,0,m_3g,0,m_4g,0,m_5g,0]^{\mathrm{T}}. \tag{15}$$

$$\mathbf{F}_s=[0,0,0,0,F_{sx3},0,F_{sx4},0,0,0,0,0,0,0,F_{sy3},0,F_{sy4},0,0,0]^{\mathrm{T}} \tag{16}$$

where F_{sx3}, F_{sx4}, F_{sy3} and F_{sy4} are nonlinear seal forces of two discs in x and y directions.

2.2. Nonlinear oil-film force

Nonlinear oil-film forces [3,4] (F_{bx5} and F_{by5}) based on the assumption of short bearings can be calculated as

$$\begin{bmatrix} F_{bx5} \\ F_{by5} \end{bmatrix}=\sigma\begin{bmatrix} f_{bx5} \\ f_{by5} \end{bmatrix}, \tag{17}$$

$$\sigma=\eta\omega\frac{D}{2}L\left(\frac{D}{2c}\right)^2\left(\frac{L}{D}\right)^2 \tag{18}$$

where f_{bx5} and f_{by5} are dimensionless nonlinear oil-film forces of the right bearing in x and y directions; η, L and D are oil viscosity, bearing length and bearing diameter respectively. The dimensionless displacements of right journal in x and y directions are given as follows:

$$\tilde{x}_5 = \frac{x_5}{c}, \quad \tilde{y}_5 = \frac{y_5}{c} \tag{19}$$

$$\begin{bmatrix} f_{bx5} \\ f_{by5} \end{bmatrix} = \frac{\left[(\tilde{x}_5 - 2\dot{\tilde{y}}_5)^2 + (\tilde{y}_5 + 2\dot{\tilde{x}}_5)^2\right]^{1/2}}{1 - \tilde{x}_5^2 - \tilde{y}_5^2} \times \begin{bmatrix} 3\tilde{x}_5 V(\tilde{x}_5, \tilde{y}_5, \alpha) - \sin\alpha G(\tilde{x}_5, \tilde{y}_5, \alpha) - 2\cos\alpha S(\tilde{x}_5, \tilde{y}_5, \alpha) \\ 3\tilde{y}_5 V(\tilde{x}_5, \tilde{y}_5, \alpha) + \cos\alpha G(\tilde{x}_5, \tilde{y}_5, \alpha) - 2\sin\alpha S(\tilde{x}_5, \tilde{y}_5, \alpha) \end{bmatrix} \tag{20}$$

where the functions V, S, G and α are respectively given in Eqs. (21)–(24):

$$V(\tilde{x}_5, \tilde{y}_5, \alpha) = \frac{2 + (\tilde{y}_5 \cos\alpha - \tilde{x}_5 \sin\alpha) G(\tilde{x}_5, \tilde{y}_5, \alpha)}{1 - \tilde{x}_5^2 - \tilde{y}_5^2}, \tag{21}$$

$$S(\tilde{x}_5, \tilde{y}_5, \alpha) = \frac{\tilde{x}_5 \cos\alpha + \tilde{y}_5 \sin\alpha}{1 - (\tilde{x}_5 \cos\alpha + \tilde{y}_5 \sin\alpha)^2}, \tag{22}$$

$$G(\tilde{x}_5, \tilde{y}_5, \alpha) = \frac{2}{(1 - \tilde{x}_5^2 - \tilde{y}_5^2)^{1/2}} \left[\frac{\pi}{2} + \arctan\frac{\tilde{y}_5 \cos\alpha - \tilde{x}_5 \sin\alpha}{(1 - \tilde{x}_5^2 - \tilde{y}_5^2)^{1/2}}\right], \tag{23}$$

$$\alpha = \arctan\left(\frac{\tilde{y}_5 + 2\dot{\tilde{x}}_5}{\tilde{x}_5 - 2\dot{\tilde{y}}_5}\right) - \frac{\pi}{2}\mathrm{sgn}\left(\frac{\tilde{y}_5 + 2\dot{\tilde{x}}_5}{\tilde{x}_5 - 2\dot{\tilde{y}}_5}\right) - \frac{\pi}{2}\mathrm{sgn}(\tilde{y}_5 + 2\dot{\tilde{x}}_5). \tag{24}$$

2.3. Nonlinear seal force

Muszynska model is used to describe the nonlinear seal force because it not only reflects the nonlinear characteristics of seal force but also describes a clear physical meaning.

$$\begin{bmatrix} F_{sxi} \\ F_{syi} \end{bmatrix} = -\begin{bmatrix} K_f - m_f \tau_f^2 \omega^2 & \tau_f \omega D_f \\ -\tau_f \omega D_f & K_f - m_f \tau_f^2 \omega^2 \end{bmatrix} \begin{bmatrix} x_i \\ y_i \end{bmatrix} - \begin{bmatrix} D_f & 2\tau_f m_f \omega \\ -2\tau_f m_f \omega & D_f \end{bmatrix} \begin{bmatrix} \dot{x}_i \\ \dot{y}_i \end{bmatrix} - \begin{bmatrix} m_f & 0 \\ 0 & m_f \end{bmatrix} \begin{bmatrix} \ddot{x}_i \\ \ddot{y}_i \end{bmatrix} \quad (i = 3, 4) \tag{25}$$

where K_f, m_f, D_f and τ_f are equivalent stiffness, equivalent mass, equivalent damping and fluid average circumferential velocity ration, respectively. These parameters are all nonlinear functions of the radial displacement of the rotor.

$$\begin{gathered} K_f = K_0(1 - e_f^2)^{-n}, D_f = D_0(1 - e_f^2)^{-n}, n = \frac{1}{2} \sim 3 (\text{such as } 1/2, 1, 3/2, 2, 5/2, 3 \text{ in Ref. [31]}); \\ \tau_f = \tau_0(1 - e_f)^b, 0 < b < 1 (\text{Refs. [18, 20]}); \quad m_f = \mu_2 \mu_3 T_f^2 \end{gathered} \tag{26}$$

where the empirical parameter n, b and τ_0 determined by types of seal are set to 2.5 (Ref. [19]), 0.5 (Ref. [20]) and 0.25 (a intermediate value between τ_0=0.2 in Ref. [19] and τ_0=0.3,0.4 in Ref. [20]), respectively. In Eq. (27), the radio of the rotor radial displacement to seal clearance e_f is defined as

$$e_f = \sqrt{x^2 + y^2}/c_f \tag{27}$$

Furthermore, K_0 and D_0 in Eq. (26) are given by Childs [15].

$$K_0 = \mu_3 \mu_0, \quad D_0 = \mu_1 \mu_3 T_f \tag{28}$$

where

$$\mu_0 = \frac{2\sigma^2}{1 + \xi + 2\sigma} E_f (1 - m_0), \quad \mu_1 = \frac{2\sigma^2}{1 + \xi + 2\sigma}\left[\frac{E_f}{\sigma} + \frac{B}{2}\left(\frac{1}{6} + E_f\right)\right], \quad \mu_2 = \frac{\sigma}{1 + \xi + 2\sigma}\left(\frac{1}{6} + E_f\right), \quad \mu_3 = \frac{\pi R_f \Delta P}{\lambda}, \quad T_f = \frac{l_f}{v} \tag{29}$$

and

$$\lambda = n_0 (R_a)^{m_0}\left[1 + \left(\frac{R_v}{R_a}\right)^2\right]^{(1 + m_0)/2}, \quad \sigma = \frac{\lambda l_f}{c_f}, \quad E_f = \frac{1 + \xi}{2(1 + \xi + 2\sigma)}, \quad B = 2 - \frac{(R_v/R_a)^2 - m_0}{(R_v/R_a)^2 + 1}, \quad R_v = \frac{R_f \omega c_f}{\upsilon}, \quad R_a = \frac{2 v c_f}{\upsilon} \tag{30}$$

Here, the parameters of Eq. (30) are as follows: ξ=0.1, n_0=0.079, m_0=−0.25 (Ref. [22]); $\upsilon = 1.5 \times \times 10^{-5}$ Pa s (dynamic viscous coefficient of air).

2.4. Dimensionless equation of motion

In order to facilitate calculation and avoid excessive truncation errors, the dimensionless transformations are given as follows:

$$\tilde{\mathbf{q}} = \frac{\mathbf{q}}{c}, \quad \tilde{x}_i = \frac{x_i}{c}, \quad \tilde{y}_i = \frac{y_i}{c} \quad (i = 1,2,3,4,5) \tag{31}$$

Through Eq. (31), dimensionless equation of Eq. (1) can be rewritten as follows:

$$\omega^2 \mathbf{M}_f \ddot{\tilde{\mathbf{q}}} + \omega(\mathbf{G}+\mathbf{C})\dot{\tilde{\mathbf{q}}} + \mathbf{K}\tilde{\mathbf{q}} = \frac{\mathbf{F}_e + \mathbf{F}_b - \mathbf{F}_g}{c} + \tilde{\mathbf{F}}_s, \tag{32}$$

$$\tilde{\mathbf{F}}_s = \begin{bmatrix} \tilde{F}_{sxi} \\ \tilde{F}_{syi} \end{bmatrix} = -\begin{bmatrix} K_f - m_f\tau_f^2\omega^2 & \tau_f\omega D_f \\ -\tau_f\omega D_f & K_f - m_f\tau_f^2\omega^2 \end{bmatrix}\begin{bmatrix} \tilde{x}_i \\ \tilde{y}_i \end{bmatrix} - \omega\begin{bmatrix} D_f & 2\tau_f m_f\omega \\ -2\tau_f m_f\omega & D_f \end{bmatrix}\begin{bmatrix} \dot{\tilde{x}}_i \\ \dot{\tilde{y}}_i \end{bmatrix} \quad (i = 3,4), \tag{33}$$

$$\mathbf{M}_f = \begin{bmatrix} \mathbf{M}_{xf} & 0 \\ 0 & \mathbf{M}_{yf} \end{bmatrix} \tag{34}$$

where

$$\mathbf{M}_{xf} = \mathbf{M}_{yf} = \mathrm{diag}[m_1, J_{d1}, m_2, J_{d2}, m_3 + m_{f3}, J_{d3}, m_4 + m_{f4}, J_{d4}, m_5, J_{d5}]. \tag{35}$$

Considering the change of mass matrix caused by seal, Eq. (10) is revised as follows:

$$\mathbf{C}_1 = \alpha \mathbf{M}_f + \beta \mathbf{K} \tag{36}$$

Eq. (32) can be solved by using numerical methods. In this paper, Newmark integration method is adopted because it is a kind of robust algorithm to solve nonlinear equations in the time domain. The spectrum cascade is used to exhibit continuous changes of frequency components of the rotor-bearing system. The rotating speed and the eccentricities of two discs are selected as control parameters, which vary with a constant step. The Poincaré map, which is a stroboscopic picture of motion in a phase plane and consists of the time series at a constant interval of T ($T=2\pi/\omega$), is adopted to indicate the nature of the system motion. The rotor orbit is used to show the axis trace moving direction. The vibration waveform is adopted to indicate the time features at some parameters.

The physical dimension of the rotor system is shown in Fig. 1a. The other parameters of the model about the bearing and seal are listed in Table 1. Assuming that the stiffness of the right bearing is the same as that of the left bearing, the first and second natural frequencies without considering seal influence can be determined as 28.6 Hz and 105 Hz approximately when the rotor is stationary. In the following Sections 3 and 4, numerical simulation will be carried out under two loading conditions of different shafts. In order to understand the vibration intensity of the rotor-bearing-seal system intuitively, the vibration responses are presented by dimensional forms and the detailed simulation condition schematic is shown in Fig. 2.

3. Simulation 1 under two loading conditions

Based on the API Standard 617 [33], the two unbalance loading conditions are determined by the modal shape of the system, as is shown in Fig. 1b. The first loading condition corresponds to in-phase unbalances of two discs and the unbalance moments are $m_3r = m_4r = 1.1838 \times 10^{-4}$ kg m, respectively. For the second loading condition, $m_3r = m_4r$ are the same as those under the first loading condition and the unbalances of two discs are out-of-phase. In this section, only vibration responses of the right bearing (the lumped mass point 5) are shown by spectrum cascade of the rotor in y direction, rotor orbits and Poincaré maps.

3.1. Simulation 1: influence of nonlinear oil-film force under two loading conditions

3.1.1. Simulation 1: vibration responses under the first loading condition

Rotating speed is one of the key parameters affecting the dynamic characteristics of the rotor system. Under the first loading condition, spectrum cascade of the rotor in y direction, rotor orbits and Poincaré maps are shown in Fig. 3, which shows the following dynamic phenomena:

(1) When the rotating speed ω approaches about double the first natural frequency (about 3000 rev/min), the first mode whirl frequency reaches the first balance resonance frequency and disappears near 3300 rev/min; the synchronous motion appears in the range of $\omega \in [3300, 4800]$ rev/min; the first mode whip appears at 4800 rev/min and the whip frequency remains close to the first critical speed, in addition, the oil whip amplitude is much higher than that of synchronous vibration.

Table 1
Model parameters of the rotor-bearing-seal system.

Parameters	Value
m_1, m_2, m_3, m_4, m_5 (kg)	0.0439, 0.02343, 0.5919, 0.5919, 0.09633
J_{p1}, J_{d1} (kg m^2)	2.957×10^{-6}, 3.196×10^{-6}
J_{p2}, J_{d2} (kg m^2)	0.2929×10^{-6}, 2.966×10^{-6}
J_{p3}, J_{d3} (kg m^2)	4.735×10^{-4}, 2.478×10^{-4}
J_{p4}, J_{d4} (kg m^2)	4.735×10^{-4}, 2.478×10^{-4}
J_{p5}, J_{d5} (kg m^2)	7.526×10^{-6}, 8.780×10^{-6}
η (Pa s)	0.04
k_{blx}, k_{bly} (N/m)	2×10^8, 2×10^8
c_{blx}, c_{bly} (N s/m)	2×10^3, 2×10^3
c, D, L (mm)	0.3, 25, 10
ξ_1, ξ_2	0.02, 0.04
ξ	0.1
R_f (mm)	43
l_f (mm)	18
c_f (mm)	1.5
v (m/s)	10
ΔP (Pa)	0.1×10^5
υ (Pa s)	1.5×10^{-5}

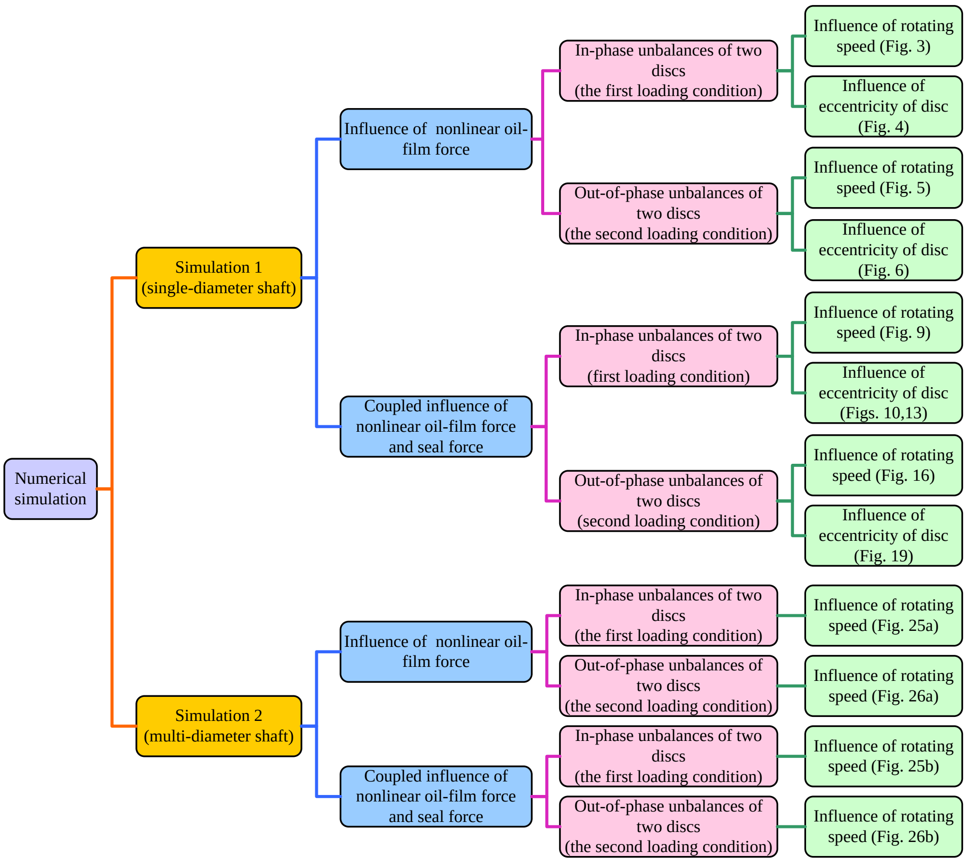

Fig. 2. Simulation condition schematic.

(2) The frequency components of the system caused by oil whip include the first whip frequency f_{n1}, rotating frequency f_r and combination frequencies of both, such as $2f_{n1}$, f_r-3f_{n1}, f_r+f_{n1}, etc.
(3) Rotor orbits and Poincaré maps at constant speeds show that the system motion is quasi-periodic at $\omega=2800$, 5000 and 12,000 rev/min.

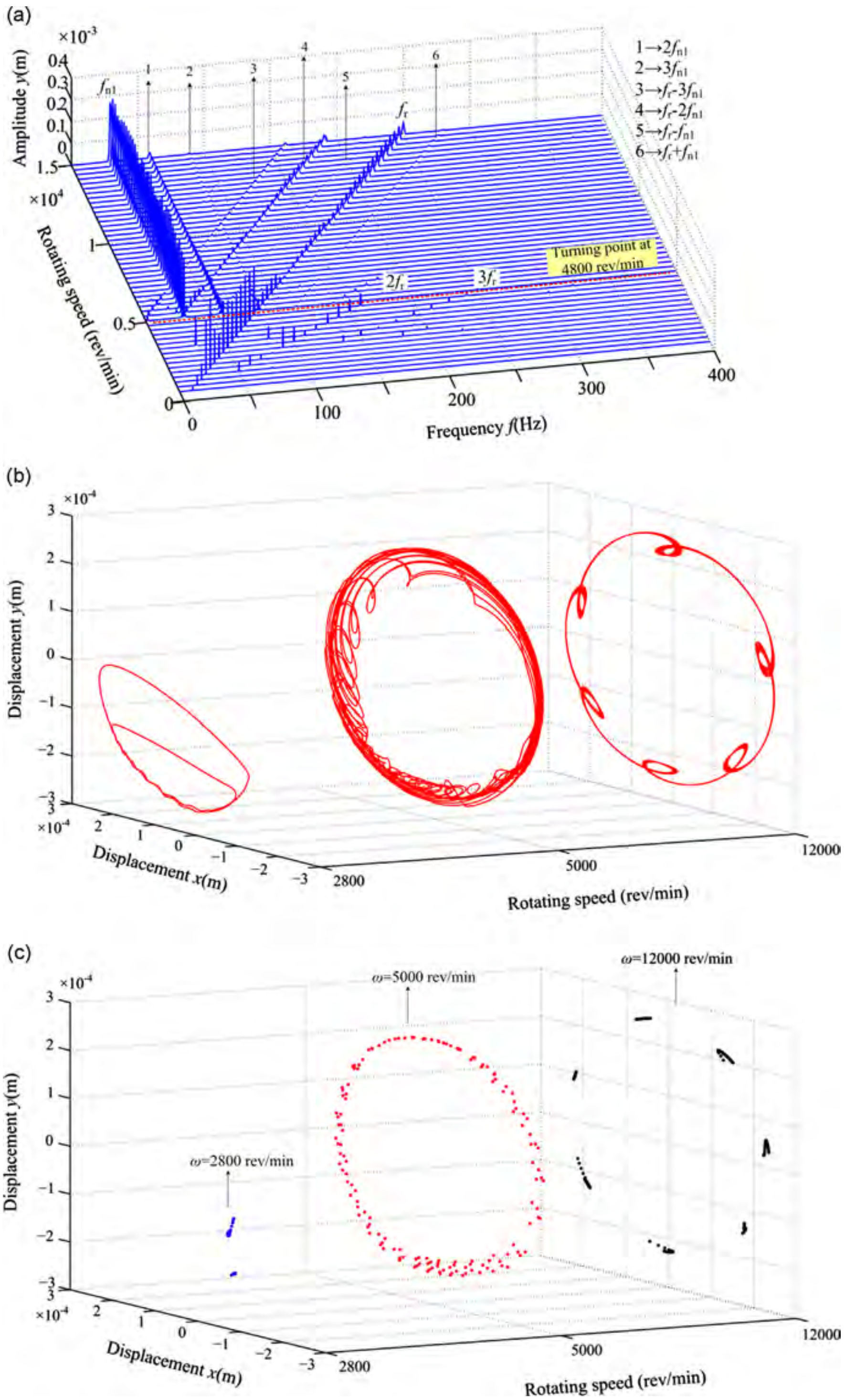

Fig. 3. Vibration response of the rotor-bearing system under the first loading condition: (a) spectrum cascade in y direction, (b) rotor orbits, and (c) Poincaré maps.

The spectrum cascades with the change of eccentricities r of two discs at 6500 and 12,000 rev/min are depicted in Fig. 4a and b, respectively. They all indicate that the amplitude of f_r increases slightly, and the amplitude of f_{n1} keeps constant with increasing eccentricity under the first loading condition. Furthermore, Fig. 4b also indicates that the amplitude of $5f_{n1}$ increases markedly compared with those of other combination frequency components.

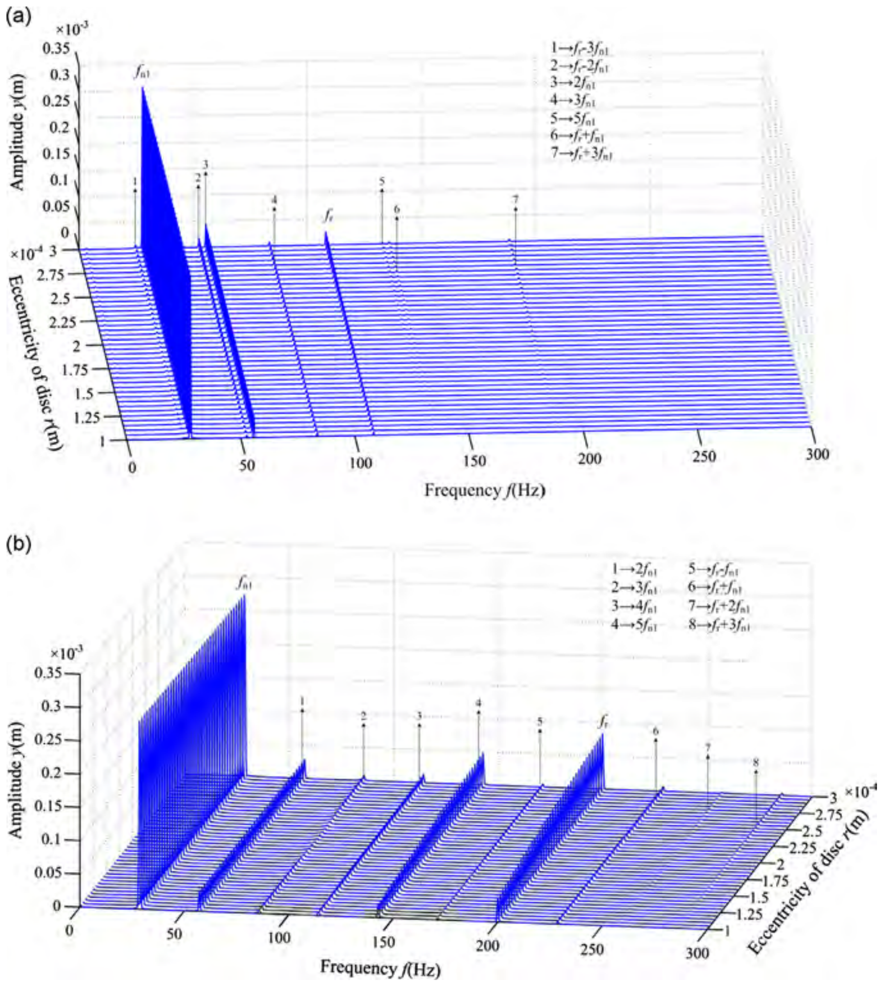

Fig. 4. Spectrum cascades of the rotor-bearing system under the first loading condition: (a) 6500 rev/min and (b) 12,000 rev/min.

3.1.2. Simulation 1: vibration responses under the second loading condition

Under the second loading condition, spectrum cascade of the rotor in y direction, rotor orbits and Poincaré maps (see Fig. 5) exhibits the following dynamic phenomena.

(1) When the rotating speed approaches about double the first natural frequency about 3000 rev/min, the half-speed oil whirl frequency reaches the first balance frequency and disappears at 3900 rev/min; the synchronous motion appears in the range of $\omega \in [3900,8700]$ rev/min; the first mode whip appears at 8700 rev/min, and the whip frequency remains close to the first critical speed of the rotor. The second mode whip appears in the range of $\omega \in [12{,}000,13{,}200]$ rev/min. It appears again and its amplitude increases sharply when $\omega \geq 14{,}100$ rev/min.

(2) The frequency components of the system in different rotating speed ranges include complicated combination frequency components about f_r, f_{n1} and f_{n2}, such as f_r-3f_{n1}, f_r-2f_{n1}, f_r-f_{n2}, etc.

(3) Rotor orbits and Poincaré maps (see Fig. 5b and c) at constant speeds shows that system motion is quasi-periodic at 3200 rev/min, period-one motion at 6500 rev/min and quasi-periodic motions determined by a closed circle in Poincaré maps at 10,000, 13,800 and 16,000 rev/min.

The spectrum cascades with the change of eccentricity at 6500 rev/min and 16,000 rev/min are depicted in Fig. 6a and b, respectively. When the rotating speed is 6500 rev/min, there is no oil-film instability and the amplitude of f_r increases slightly. Fig. 6b shows that f_{n1} and f_r are obvious and the amplitude of f_{n1} is maximal in the range of $r \in [0.1, 0.16]$ mm. However, f_{n2} and f_r are dominant and the amplitude of f_{n2} is maximal in the range of $r \in [0.16, 0.255]$ mm. The above analysis shows that the self-excited vibration energy of the first mode whip can be switched to that of the second mode whip under some eccentricities. The amplitudes of f_{n1} and f_{n2} decrease sharply and the continuous spectra between f_r-f_{n2} and

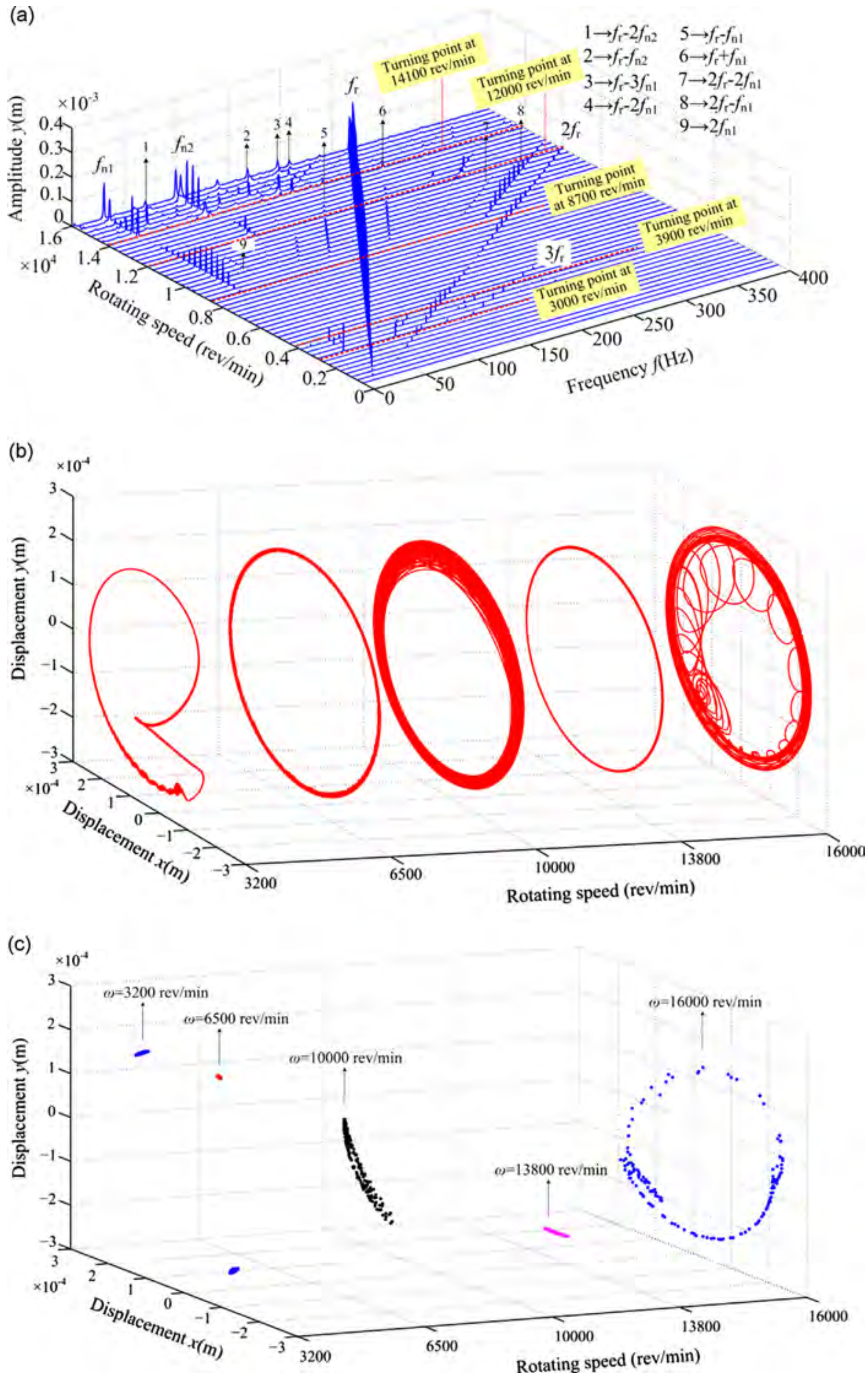

Fig. 5. Vibration response of the rotor-bearing system under the second loading condition: (a) spectrum cascade in y direction; (b) rotor orbits; and (c) Poincaré maps.

f_r can be observed in the range of $r \in [0.255,\ 0.29]$ mm. Moreover, the amplitude of f_r increases slightly when $r \le 0.29$ mm. However, the amplitude of f_r increases sharply because of the disappearance of oil-film instability when $r > 0.29$ mm.

Vibration waveforms at $\omega = 16{,}000$ rev/min under three eccentricities of $r = 0.125$, 0.24 and 0.28 mm are illustrated in Fig. 7. The rotor orbits and the Poincaré maps under different r are depicted in Fig. 8. These figures indicate the

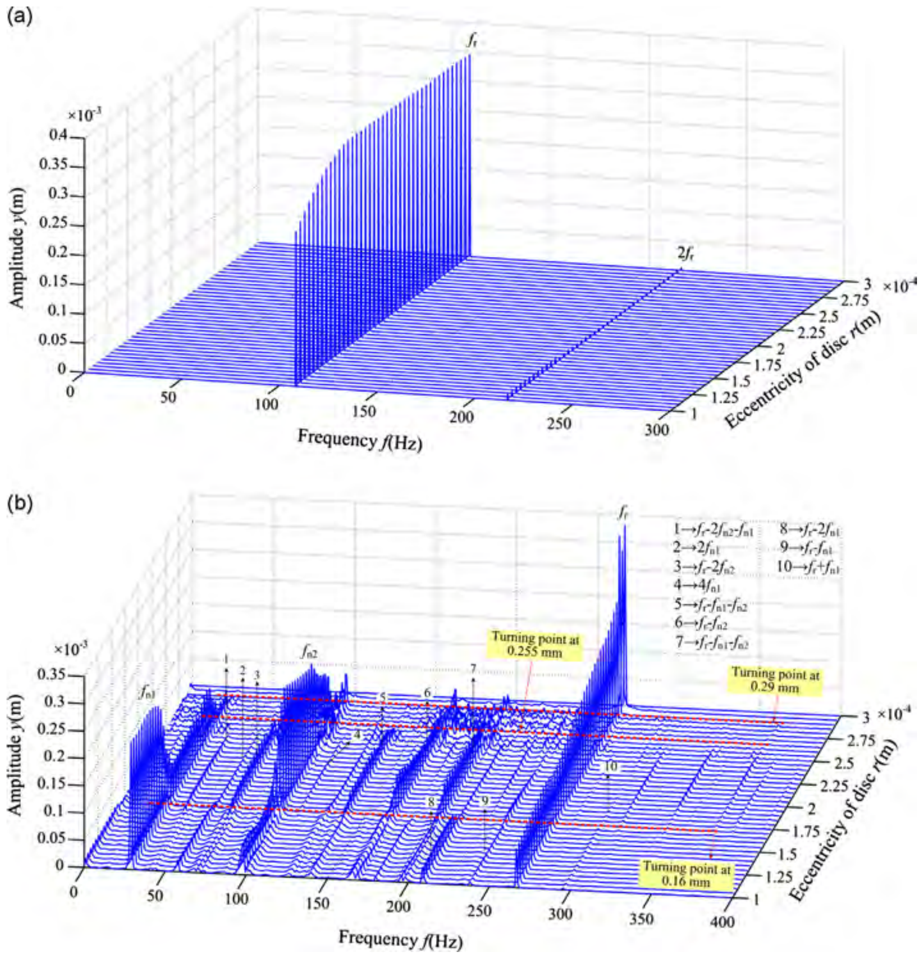

Fig. 6. Spectrum cascades of the rotor-bearing system under the second loading condition: (a) 6500 rev/min and (b) 16,000 rev/min.

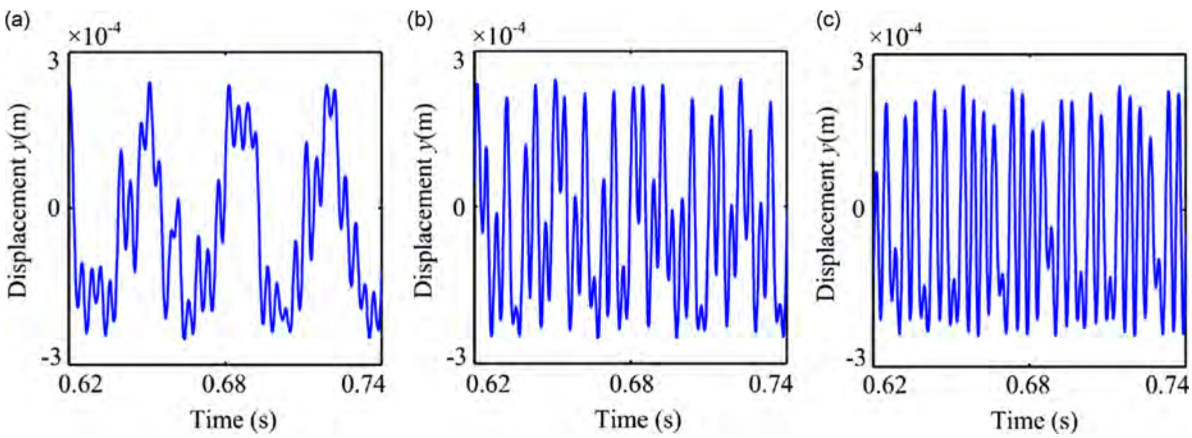

Fig. 7. Vibration waveforms at 16,000 rev/min: (a) r=0.125 mm, (b) r=0.24 mm, and (c) r=0.28 mm.

transformation process from oil-film instability to period-one motion with the changing r. Rotor orbit (see Fig. 8a) change from irregular motion caused by the oil whip to elliptical orbit with period-one motion, and the complicated motion forms can also be observed through irregular points in Poincaré maps (see Fig. 8b)

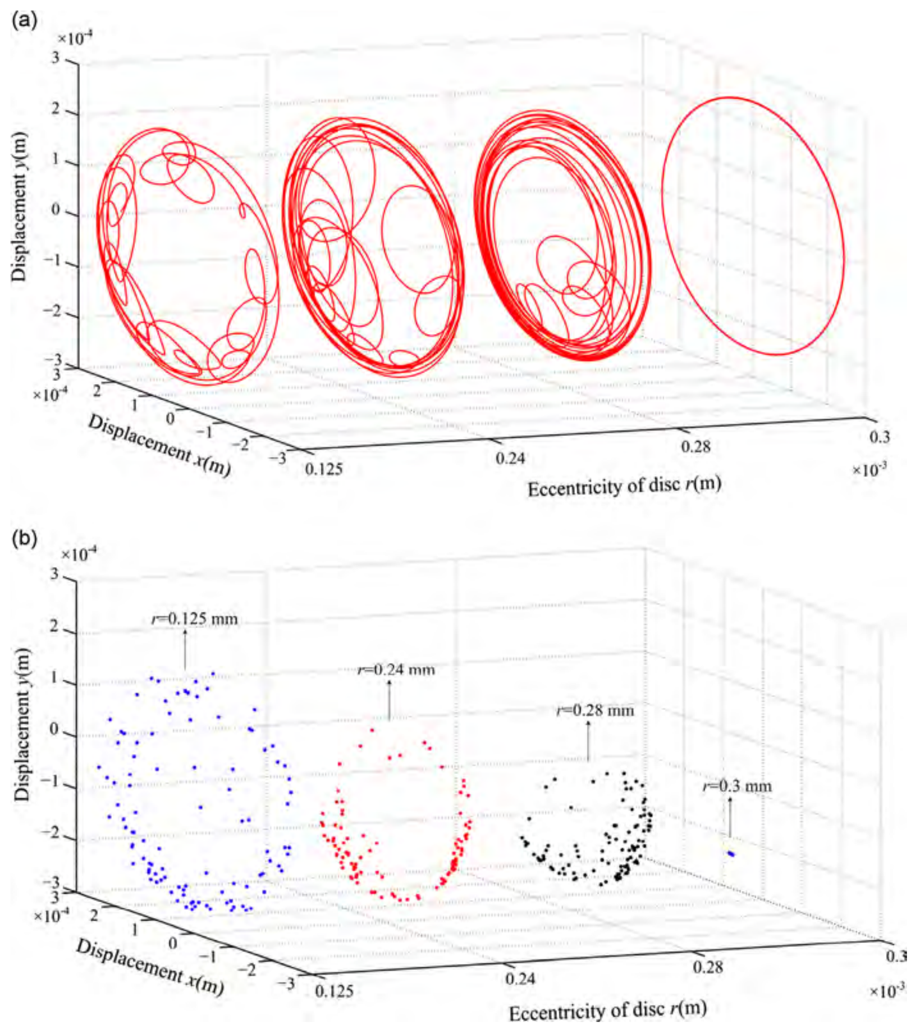

Fig. 8. Rotor orbits and Poincaré maps of the rotor-bearing system at 16,000 rev/min: (a) rotor orbits and (b) Poincaré maps.

3.2. Simulation 1: coupled influence of nonlinear oil-film force and seal force under two loading conditions

3.2.1. Simulation 1: vibration responses under the first loading condition

Under the first loading condition, spectrum cascade of the rotor-bearing-seal system in y direction, rotor orbits and Poincaré maps (see Fig. 9), which exhibits the following dynamic phenomena:

(1) The first oil whip does not appear until 6700 rev/min and its frequency is slightly greater than that in Fig. 3a. Meanwhile, the frequency components of the system include the first mode whip frequency f_{n1}, rotating frequency f_r and combination frequencies of both, such as $2f_{n1}$, $3f_{n1}$, $4f_{n1}$, $5f_{n1}$, f_r–$5f_{n1}$, f_r–$4f_{n1}$, f_r–$3f_{n1}$, f_r–$2f_{n1}$, etc.

(2) Rotor orbits and Poincaré maps (see Fig. 9b and c) show that the system motion is period-one at 2800 rev/min and 5000 rev/min and quasi-periodic motion at 12,000 rev/min, which can be determined by a closed circle in Poincaré maps.

The spectrum cascade at 6500 rev/min (see Fig. 10), which indicates the transformation process from instability to stability with the changing eccentricity r. The amplitude of f_{n1} is maximal (the maximum value is 0.1839 mm) at $r=0.1$ mm and decreases to the value of 0.1539 mm at $r=0.12$ mm, hereafter reduces sharply and disappears at $r=0.2$ mm. Vibration waveforms at $\omega=6500$ rev/min are illustrated in Fig. 11 under three eccentricities of $r=0.12$ mm, 0.15 mm and 0.22 mm. The rotor orbits and the Poincaré maps under different r are depicted in Fig. 12, which shows that the rotor motion is from quasi-periodic to period-one.

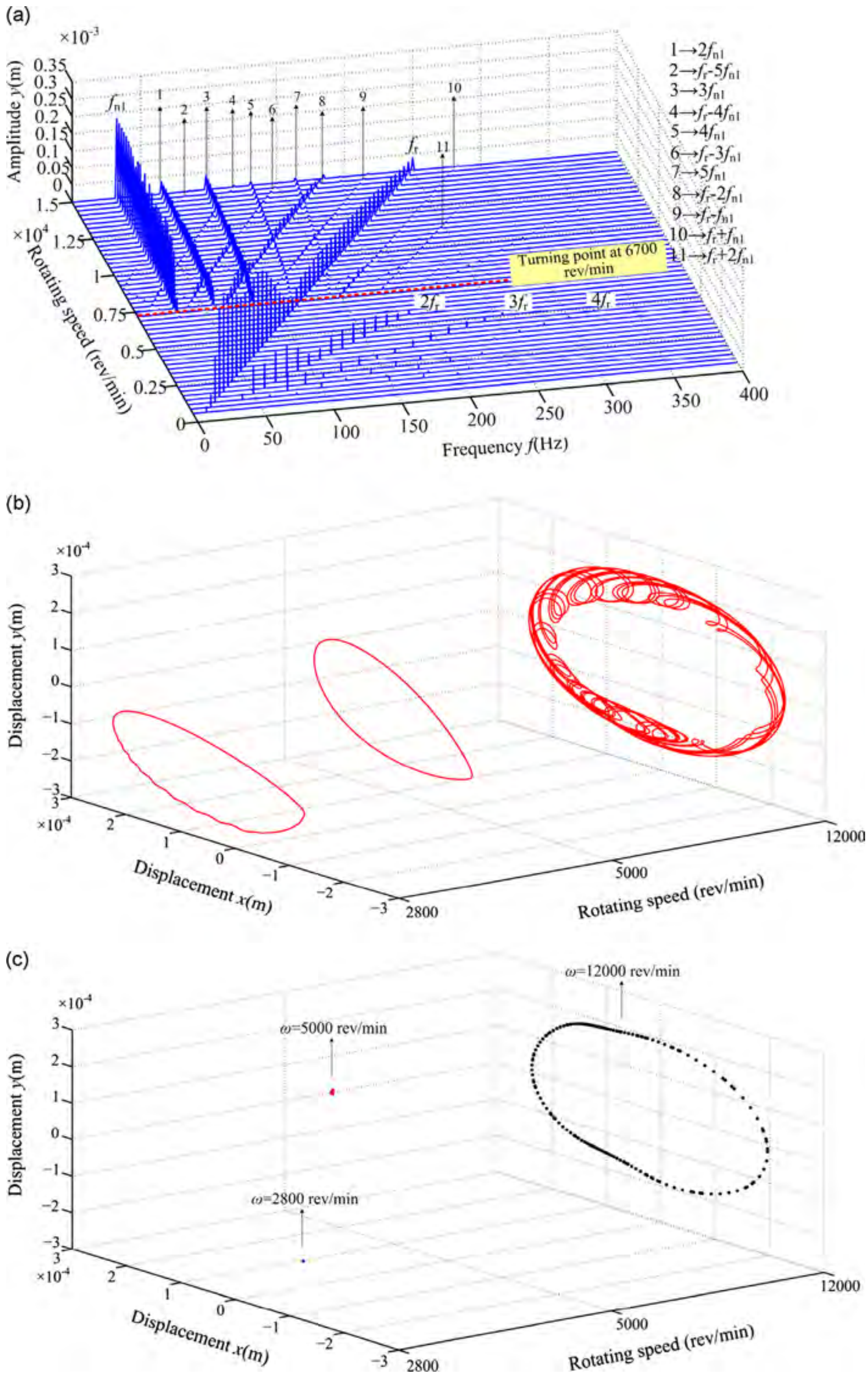

Fig. 9. Vibration response of the rotor-bearing-seal system under the first loading condition: (a) spectrum cascade in y direction, (b) rotor orbits, and (c) Poincaré maps.

The spectrum cascade at 12,000 rev/min (see Fig. 13) indicates that the combination frequency components about f_{n1} and f_r, such as $2f_{n1}$, f_r-4f_{n1}, etc., appear in the range of $r\in[0.1, 0.29]$ mm. Some new combination components, such as 24.05 Hz, 54.51 Hz, 115 Hz, etc., can be observed in the range of $r\in[0.29, 0.3]$ mm besides those in the range of $r\in[0.1, 0.29]$ mm. Vibration waveforms under three eccentricities of $r=0.1$, 0.2 and 0.3 mm at $\omega=12{,}000$ rev/min are illustrated in Fig. 14. Rotor orbits and Poincaré maps under different r are depicted in Fig. 15, which shows that system motion becomes more complicated and unstable with the increasing eccentricity r.

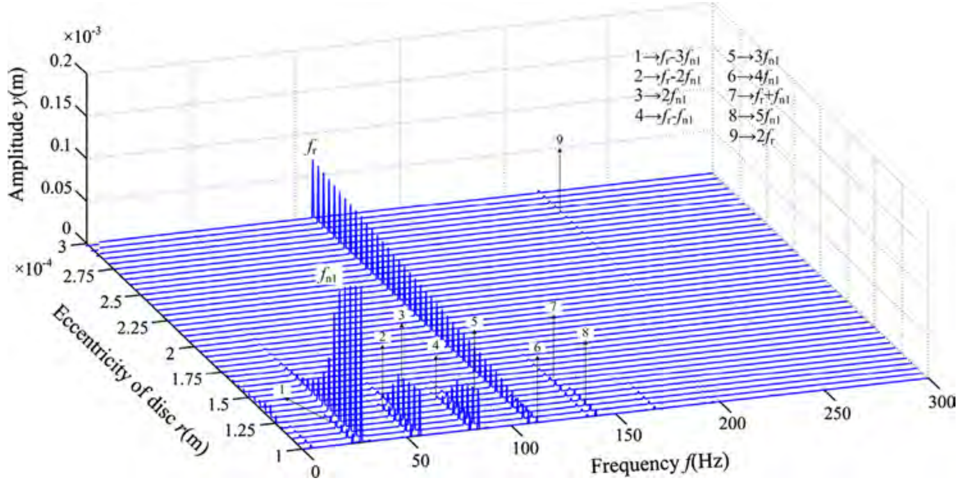

Fig. 10. Spectrum cascade of the rotor-bearing-seal system in y direction at 6500 rev/min.

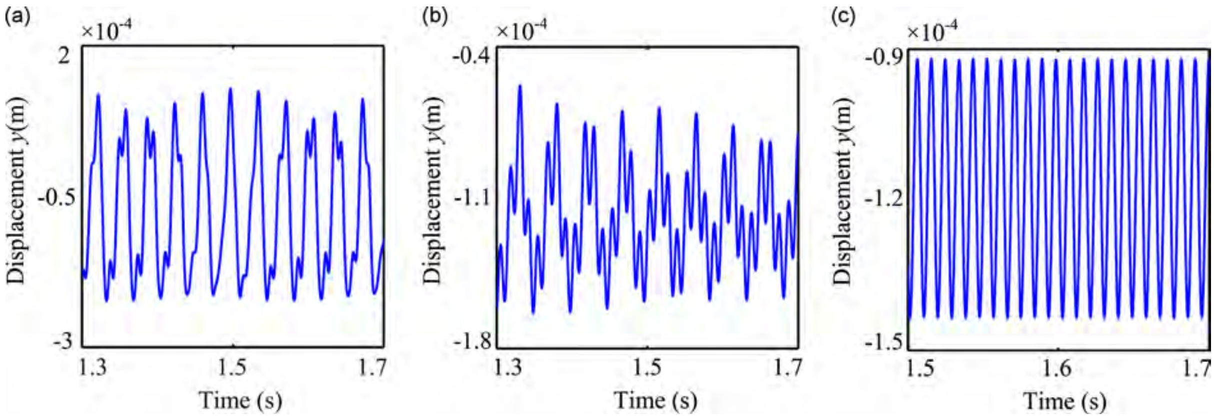

Fig. 11. Vibration waveforms at 6500 rev/min: (a) $r=0.12$ mm, (b) $r=0.15$ mm, and (c) $r=0.22$ mm.

3.2.2. Simulation 1: vibration responses under the second loading condition

Under the second loading condition, spectrum cascade of the rotor-bearing-seal system in y direction is shown in Fig. 16a. The quasi-periodic motion (regular combination frequency components about f_r can be observed, such as low frequency components 50.29 Hz and 54.71 Hz at $f_r=95$ Hz, 38.08 Hz and 56.92 Hz at $f_r=105$ Hz, respectively) appears in the range of $\omega\in[5700,7200]$ rev/min and displaced by synchronous motion in the range of $\omega\in[7200,13,500]$ rev/min. The first mode whip appears again at $\omega=13,500$ rev/min and the whip frequency is slightly greater than that in Fig. 5a. The second mode whip appears in the range of $\omega\in[14,130,14,790]$ rev/min (see Fig. 16b). The frequency components of the system in different ranges of rotating speed include complicated combination frequency components about f_r, f_{n1} and f_{n2}, such as $f_r–3f_{n1}$, $f_r–2f_{n1}$, $f_r–f_{n1}$, $f_{n1}+f_{n2}$, etc.

Vibration waveforms (see Fig. 17), rotor orbits (see Fig. 18a) and Poincaré maps (see Fig. 18b) at constant speeds show that system motion is quasi-periodic at $\omega=3200$ rev/min, period-one at $\omega=10,000$ rev/min and quasi-periodic at $\omega=6500$, 13,800 and 16,000 rev/min.

The spectrum cascade (see Fig. 19a) at 6500 rev/min indicates that the oil-film instability does not appear in the range of $r\in[0.1, 0.12]$ mm. The first mode whirl f_{n1} appears and increases from 33.87 Hz at $r=0.12$ mm to 70.12 Hz at $r=0.3$ mm in the range of $r\in[0.12, 0.3]$ mm. The instability features mentioned above at $\omega=6500$ rev/min are different from those in Fig. 6a. The spectrum cascade (see Fig. 19b) at 16,000 rev/min shows that f_{n1} and f_r are obvious and the amplitude of f_{n1} is largest in the range of $r\in[0.1, 0.225]$ mm. However, f_{n2} and f_r are dominant and the amplitude of f_{n2} is maximal in the range of $r\in[0.225, 0.255]$ mm. The above analysis shows that the self-excited vibration energy of the first mode whip can be switched to that of the second mode whip under some eccentricities. The amplitudes of f_{n1} and f_{n2} decrease sharply and the continuous spectra between $f_r–f_{n2}$ and f_r can be observed in the range of $r\in[0.255, 0.29]$ mm. The amplitude of f_r increases slightly when $r\leq0.29$ mm, however, increases sharply because of the disappearance of oil-film instability when $r>0.29$ mm. Except that f_{n1} and f_{n2} are slightly greater than those in Fig. 6b, other instability features in Fig. 19b are similar to those in Fig. 6b.

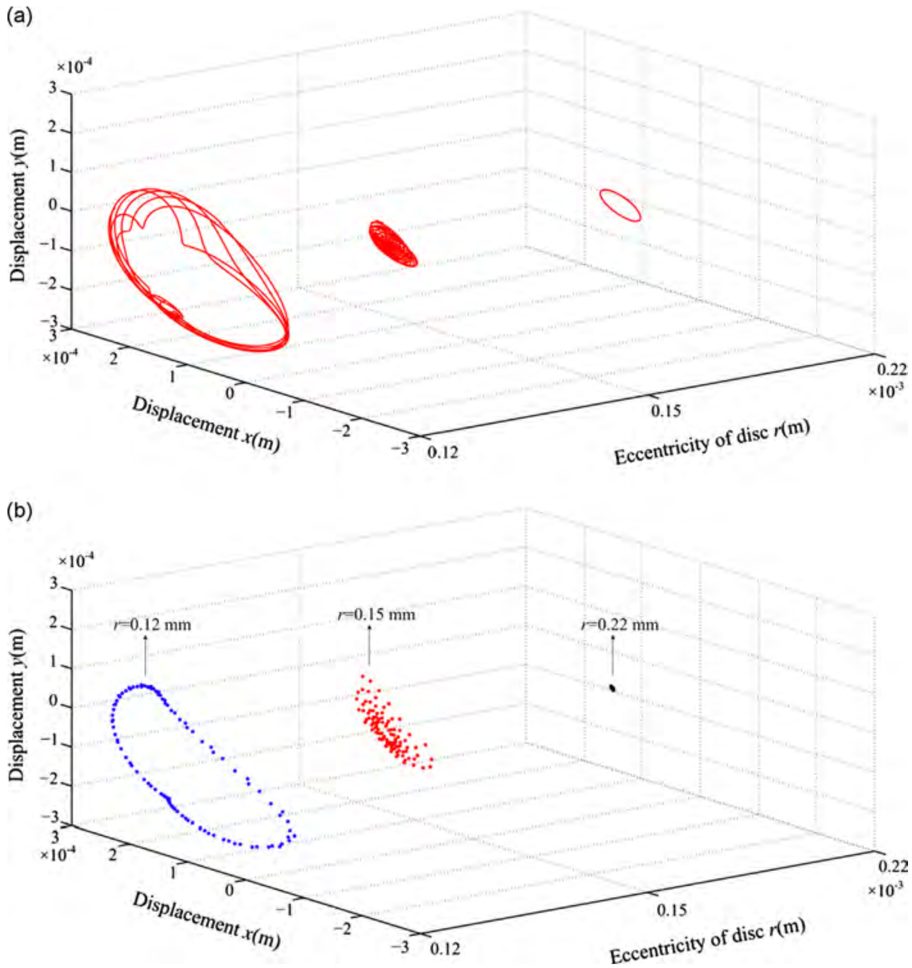

Fig. 12. Rotor orbits and Poincaré maps of the rotor-bearing-seal system at 6500 rev/min: (a) rotor orbits and (b) Poincaré maps.

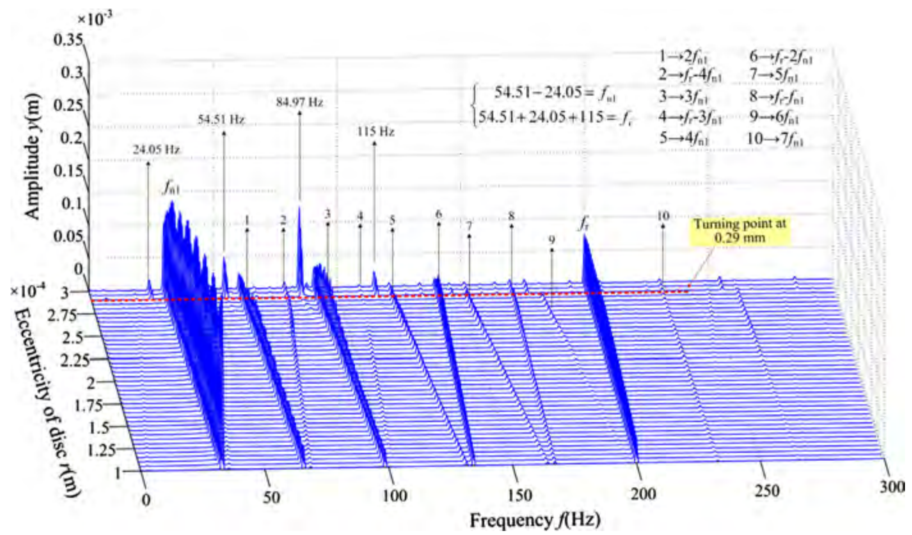

Fig. 13. Spectrum cascades in y direction of the rotor-bearing-seal system at 12,000 rev/min.

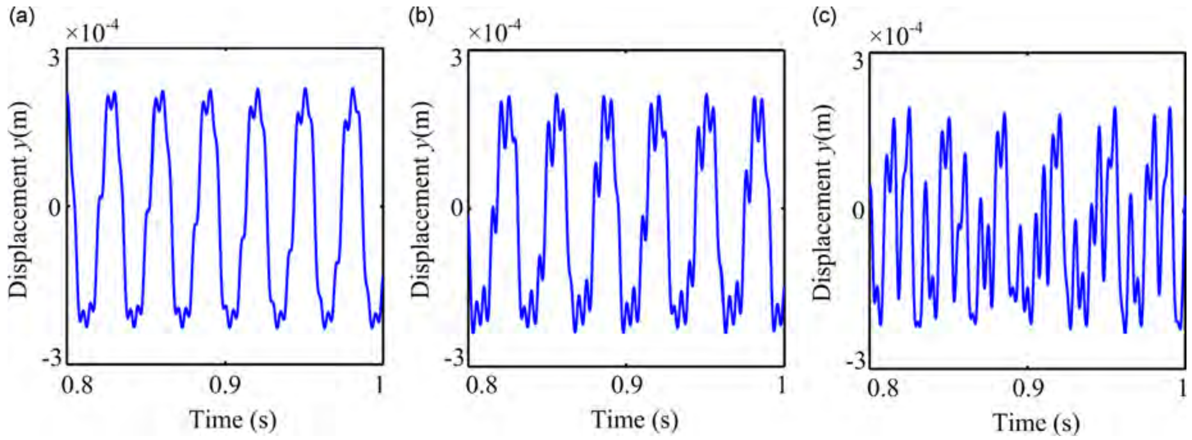

Fig. 14. Vibration waveforms at 12,000 rev/min: (a) $r=0.1$ mm, (b) $r=0.2$ mm, and (c) $r=0.3$ mm.

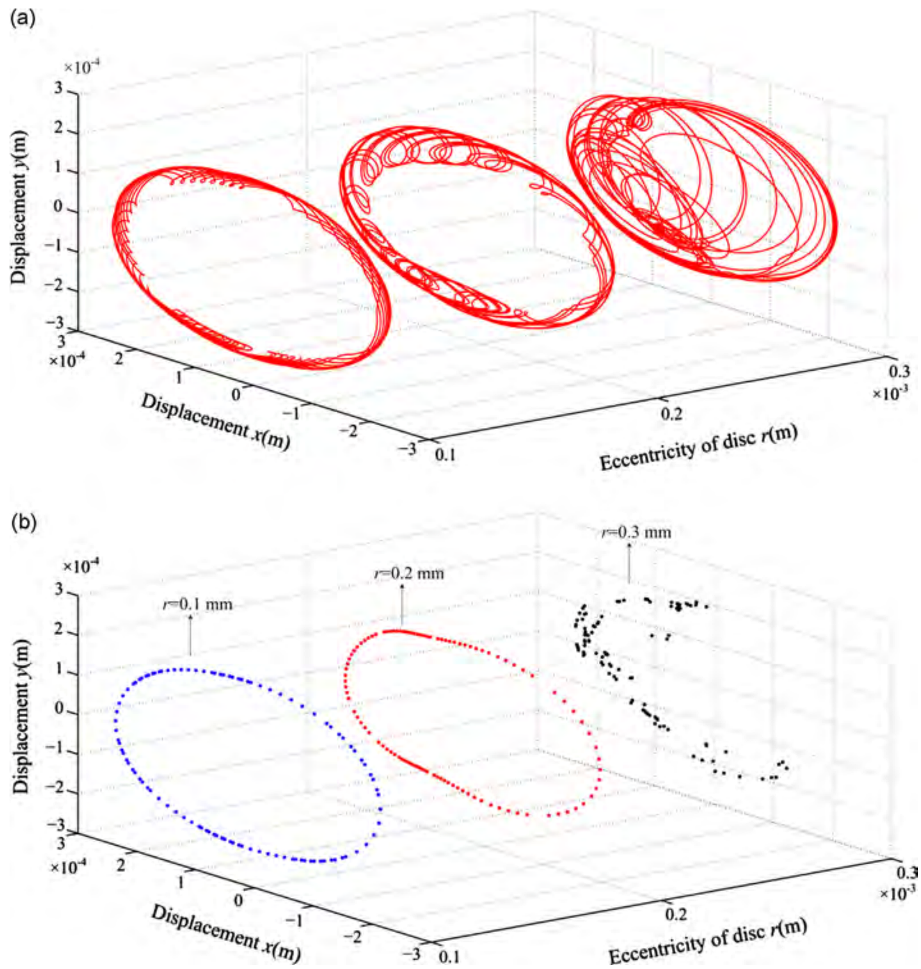

Fig. 15. Rotor orbits and Poincaré maps of the rotor-bearing-seal system at 12,000 rev/min: (a) rotor orbits and (b) Poincaré maps.

Vibration waveforms at $\omega=16{,}000$ rev/min under three eccentricities of $r=0.125$ mm, 0.24 mm and 0.28 mm are illustrated in Fig. 20. The rotor orbits and the Poincaré maps under different r are depicted in Fig. 21. System motions shown in Figs. 20 and 21 are similar to those in Figs. 6 and 8.

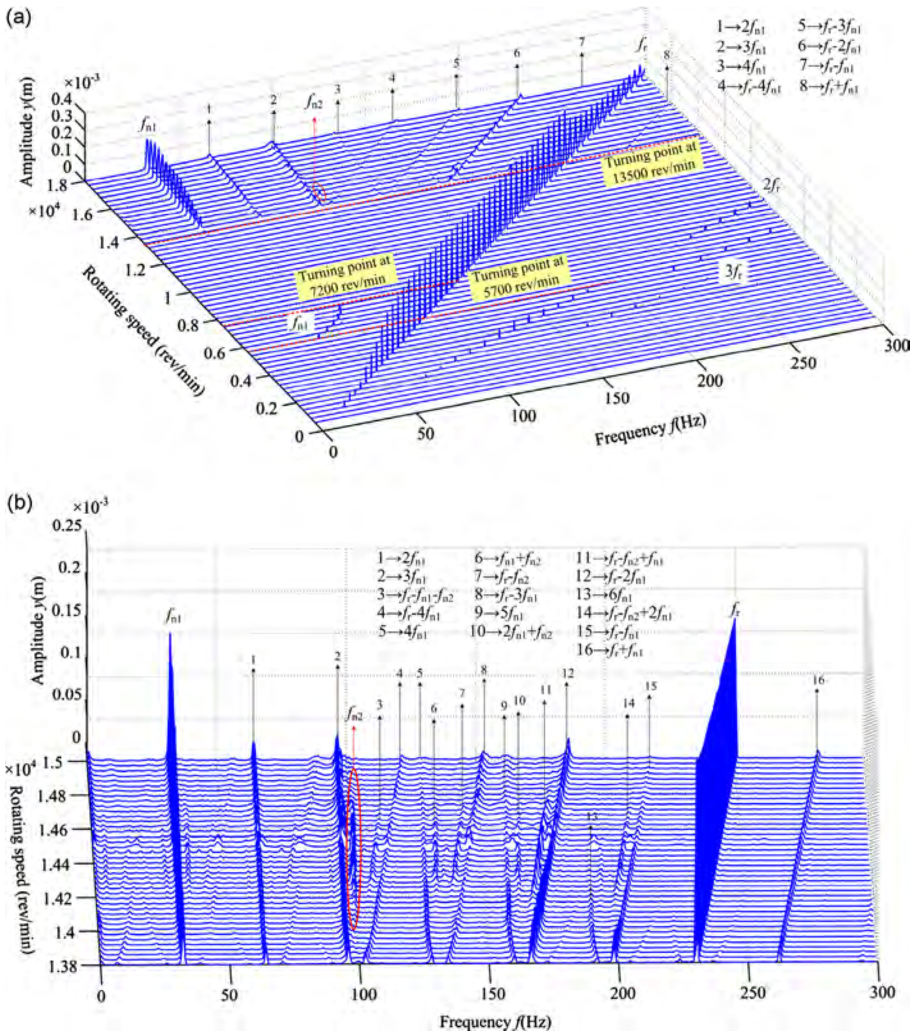

Fig. 16. Spectrum cascades of the rotor-bearing-seal system under the second loading condition: (a) spectrum cascade in the range of $\omega \in [600,18,000]$ rev/min, and (b) elaborate spectrum cascade in the range of $\omega \in [13,800,15,000]$ rev/min.

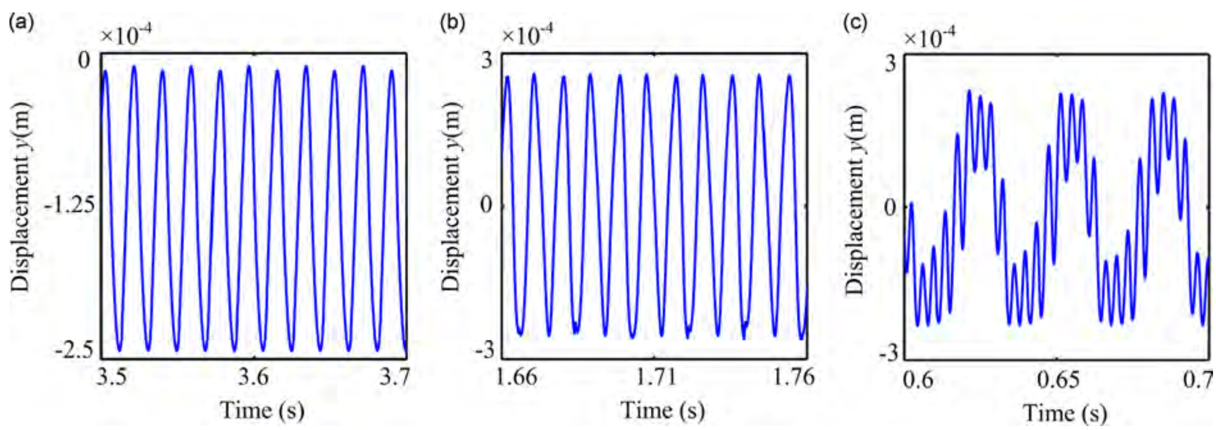

Fig. 17. Vibration waveforms: (a) $\omega = 3200$ rev/min, (b) $\omega = 6500$ rev/min, and (c) $\omega = 16,000$ rev/min.

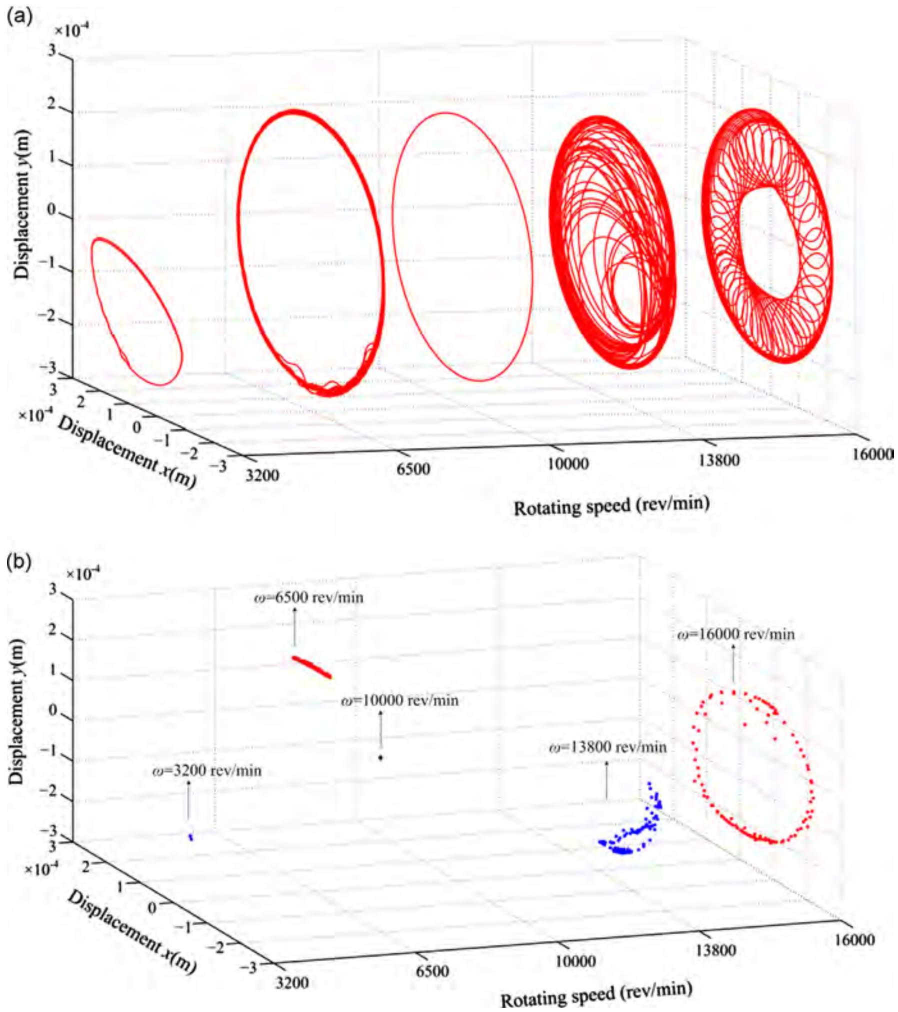

Fig. 18. Rotor orbits and Poincaré maps of the rotor-bearing-seal system under the second loading condition: (a) rotor orbits and (b) Poincaré maps.

3.3. Discussion on the results of simulation 1

In this paper, the first mode instability includes the first mode whirl and whip (oil whip evolves from half-speed whirl). When the rotating speed increases to about twice its first balance resonance, the first mode whirl frequency is close to the first natural frequency of the rotor. After that the mode whirl will be replaced by the first mode whip. Similarly, when the rotating speed increased to approximately twice its second critical speed, the second mode whip appears. As is shown in Figs. 3a and 9a, the first loading condition mainly excites the first mode instability, however, the second loading condition can excite the first and second mode instabilities (see Figs. 5a and 16).

Under the first loading condition, the first mode instability threshold in the rotor-bearing system increases from 4800 rev/min to 6700 rev/min in rotor-bearing-seal system. Combination frequency components (related to f_r and f_{n1}) of the latter become more complicated than those of the former when the rotating speed and eccentricities of two discs increase. System motion of the latter changes from quasi-periodic to period-one with increasing eccentricities of two discs at $\omega=6500$ rev/min (see Fig. 10) and the frequency components at $\omega=12{,}000$ rev/min become more complicated at some eccentricities of disc (see Fig. 13). However the former is always a stable quasi-periodic motion at $\omega=6500$ and 12,000 rev/min (see Fig. 4).

Under the second loading condition, many first and second mode instability regions (see Fig. 5a) in the rotor-bearing system appear alternatively. Only two instability regions (see Fig. 16a) can be observed in the rotor-bearing-seal system. One of them corresponds to quasi-periodic motion and the other indicates the first mode whip and slight second mode whip (see Fig. 16b). Compared with the rotor-bearing system, the instability speed is postponed and some new combination frequency components only related to f_r appear in the range of $\omega\in[5700,7200]$ rev/min in the rotor-bearing-seal system. Furthermore, the first and second mode instability are dominant in different range of eccentricities of the disc(

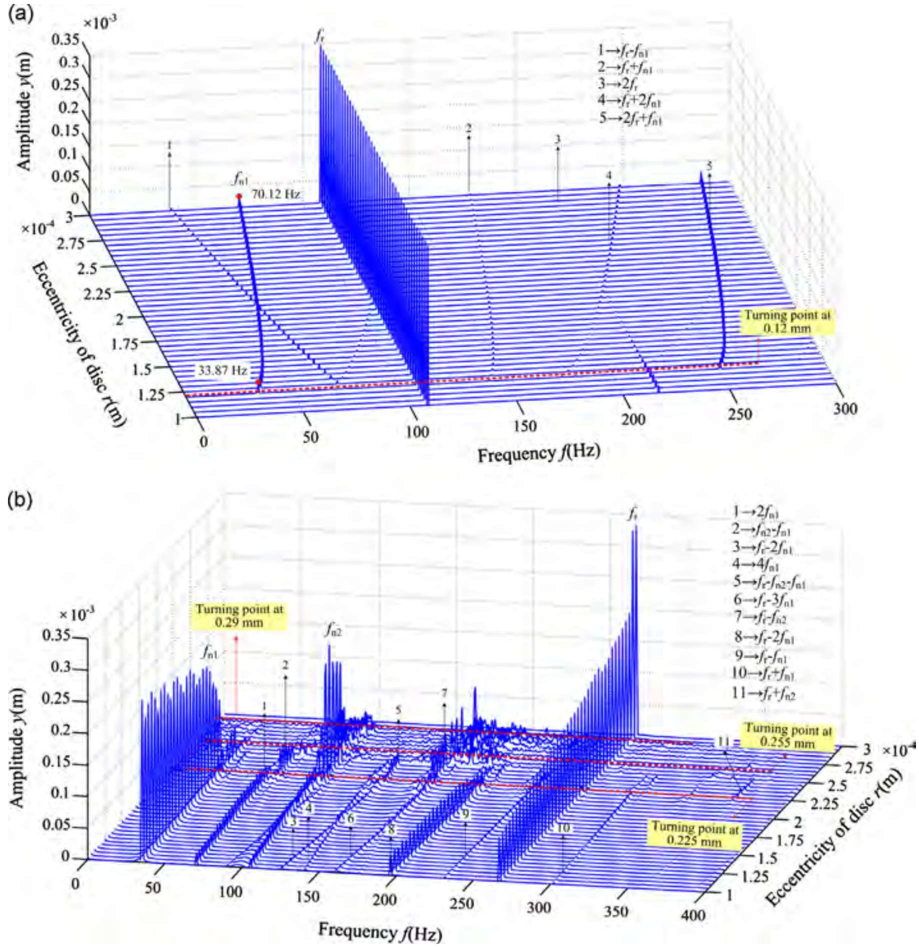

Fig. 19. Spectrum cascades of the rotor-bearing-seal system under the second loading condition: (a) 6500 rev/min and (b) 16,000 rev/min.

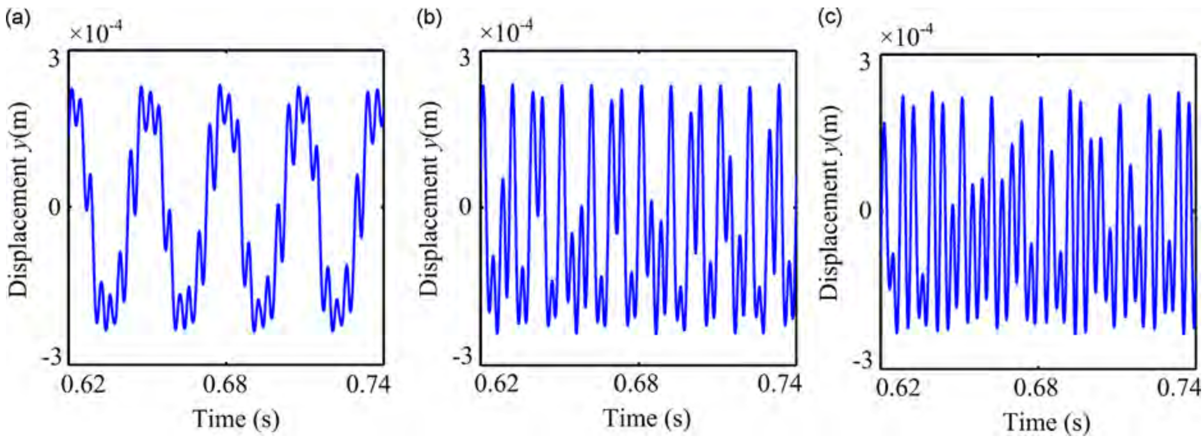

Fig. 20. Vibration waveforms at 16,000 rev/min: (a) $r=0.125$ mm, (b) $r=0.24$ mm, and (c) $r=0.28$ mm.

see Figs. 6b and 19b), which shows that the self-excited vibration energy of the first mode whip can be switched to that of the second mode whip under some eccentricities of two discs.

By the spectrum cascade comparison including and excluding the seal effect, it can be observed that the seal force can restrain the occurrence of the first and second mode instabilities. The added mass, added stiffness and added damping coefficients caused by nonlinear seal force may contribute to this phenomenon. Under two loading conditions, the equivalent stiffnesses of right disc in x direction and cross stiffnesses in x and y directions at $\omega=1706$ and 6518 rev/min are

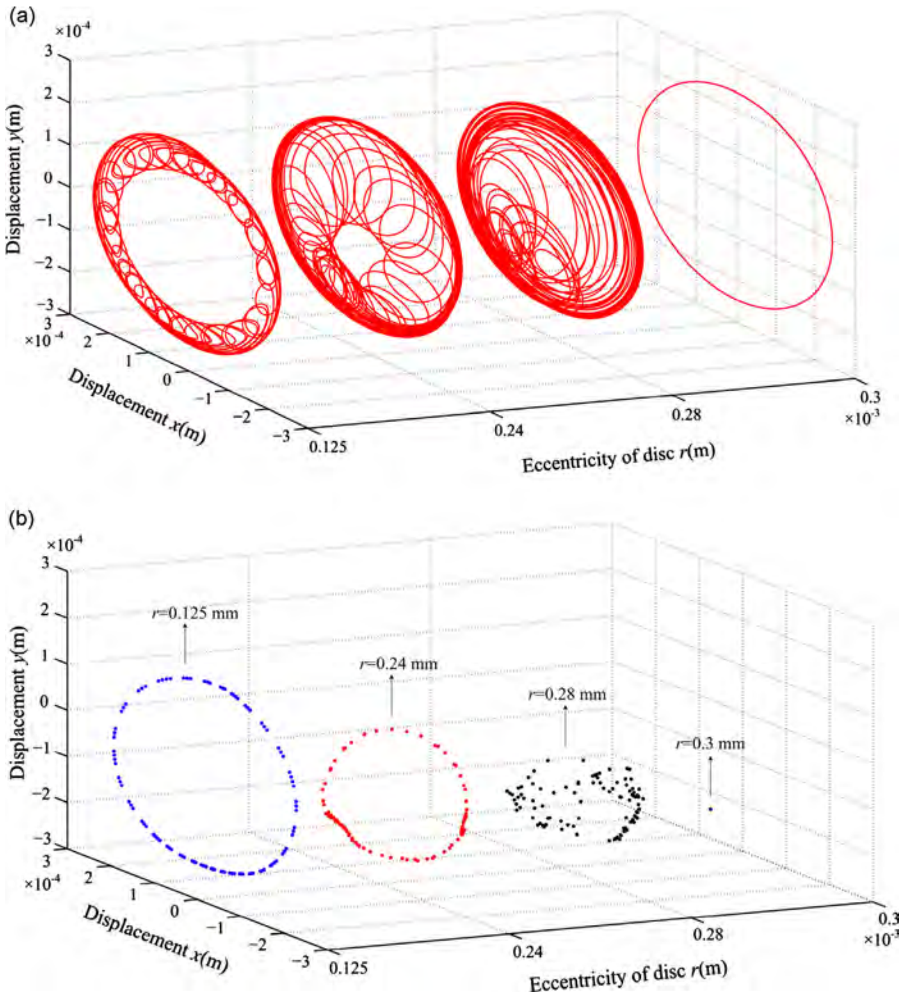

Fig. 21. Rotor orbits and Poincaré maps of the rotor-bearing-seal system at 16,000 rev/min: (a) rotor orbits and (b) Poincaré maps.

shown in Fig. 22. The average equivalent masses and stiffnesses of right disc obtained by Fig. 22 are listed in Table 2. Assuming that the stiffness of the right bearing is the same as that of the left bearing, the first two natural frequencies (see Table 3) can be determined by considering the effects of average equivalent stiffnesses (see Table 2) caused by seal at $\omega = 1706$ and 6518 rev/min.

Considering the changing average equivalent masses and stiffnesses with rotating speeds caused by seal, amplitude frequency responses including and excluding seal influence under two loading conditions are shown in Fig. 23, which shows that the seal force not only changes the critical instability speed slightly but restrains resonance responses under two loading conditions. Because the equivalent stiffness caused by seal increases with the increasing eccentricity ratio (disc radial displacement to radial clearance), the equivalent stiffness will increase sharply under instability conditions (see right figure in Fig. 22b). We have reason to believe that stiffnesses and masses caused by the nonlinear seal force can increase the first natural frequency, and then improve the first mode instability threshold significantly. However, the second natural frequency changes little by the added stiffnesses and masses of two discs caused by seal, so the nonlinear seal force has a minor effect on the second mode instability threshold.

4. Simulation 2 under two loading conditions

In order to validate the universality of the results obtained in Section 3, the shaft of the previous rotor-bearing system is changed into a multi-diameter shaft with three different shaft sections, moreover, the mass of the left disc is increased by 20 percent. The physical dimensions of the new rotor system are shown in Fig. 24. The other parameters of the model, which are different from those of the previous model, are listed in Table 4. The first and second natural frequencies in stationary state can be determined as 44 Hz and 147.5 Hz approximately, which are obtained by previous method.

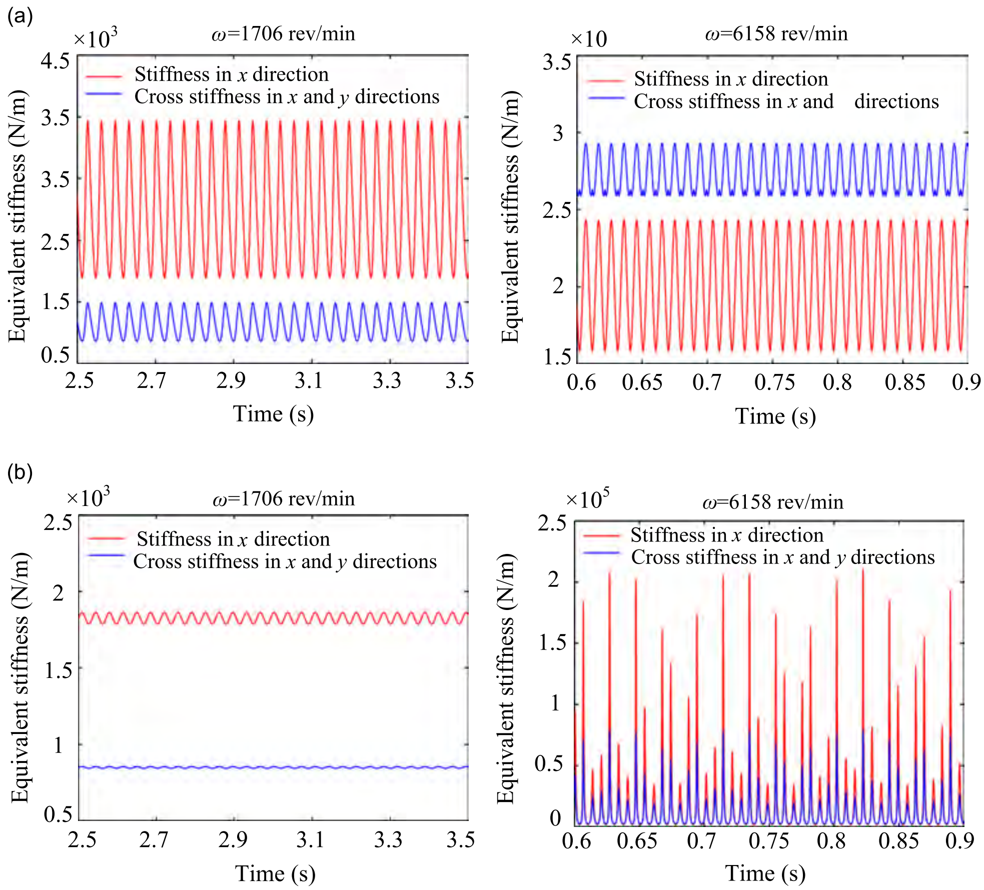

Fig. 22. Equivalent stiffnesses of the right disc under two loading conditions: (a) the first loading condition and (b) the second loading condition.

Table 2
Equivalent masses and stiffnesses of right disc.

Two loading conditions	Rotating speed (rev/min)	Equivalent mass (kg)	Average equivalent stiffness (kN/m)			
			k_{xx}	k_{xy}	k_{yx}	k_{yy}
Condition 1	1706	0.021	3.006	1.134	−1.134	3.006
Condition 1	6158	0.018	2.005	2.727	−2.727	2.005
Condition 2	1706	0.021	1.825	0.8494	−0.8494	1.825
Condition 2	6158	0.018	19.23	10.67	−10.67	19.23

Table 3
The first two natural frequencies under two loading conditions.

Two loading conditions	Rotating speed (rev/min)	The first natural frequency (Hz)	The second natural frequency (Hz)
Condition 1	1706	29.80	103.44
Condition 1	6158	29.46	103.60
Condition 2	1706	29.25	103.34
Condition 2	6158	33.88	104.35

Spectrum cascades (lumped mass point 9) of right bearing in the rotor-bearing system (see Figs. 25a and 26a) and spectrum cascades (lumped mass point 9) in the rotor-bearing-seal system (see Figs. 25b and 26b) under two loading conditions exhibit the following dynamic phenomena:

(1) Under the first loading condition, for the rotor-bearing system, the first mode whirl appears in the range of $\omega \in [3600,5400]$ rev/min, then is replaced by the first mode whip when $\omega > 5400$ rev/min and the corresponding whip

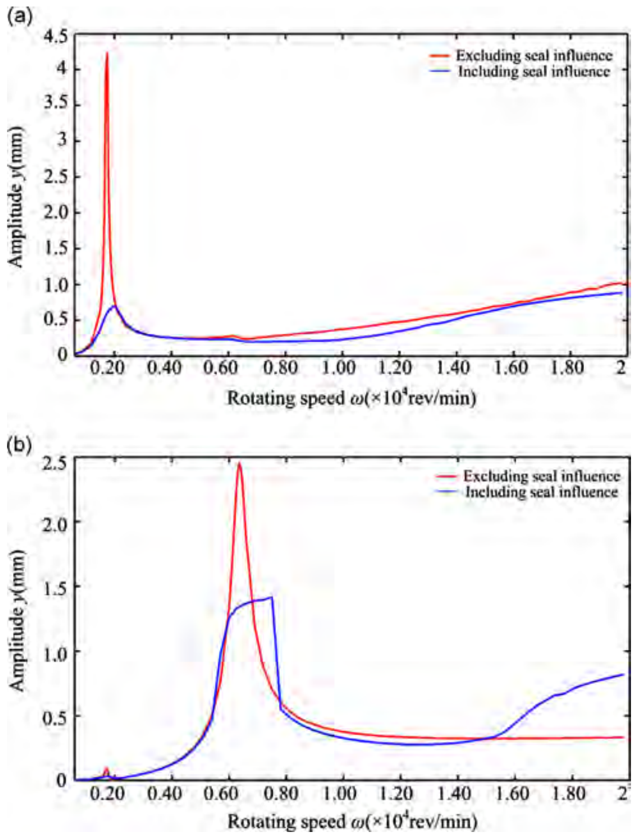

Fig. 23. Amplitude frequency responses including and excluding seal influences under two loading conditions: (a) the first loading condition and (b) the second loading condition.

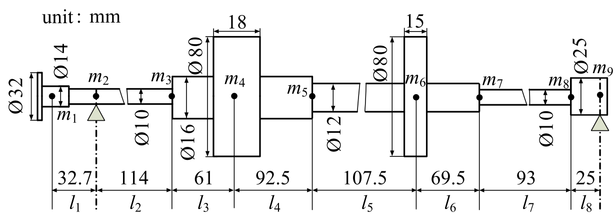

Fig. 24. Physical dimensions of a rotor-bearing system with a multi-diameter shaft.

Table 4
Model parameters of the rotor-bearing system simulated by nine lumped mass points.

Parameters	Value
m_1, m_2, m_3, m_4, m_5, m_6, m_7, m_8, m_9 (kg)	0.0408, 0.0418, 0.1066,0.75, 0.1946, 0.637, 0.0861, 0.0572, 0.058
J_{p1}, J_{d1} (kg m^2)	2.965×10^{-6}, 3.2045×10^{-6}
J_{p2}, J_{d2} (kg m^2)	0.5231×10^{-6}, 1.6244×10^{-5}
J_{p3}, J_{d3} (kg m^2)	2.5663×10^{-6}, 1.0513×10^{-4}
J_{p4}, J_{d4} (kg m^2)	5.7086×10^{-4}, 3.1366×10^{-4}
J_{p5}, J_{d5} (kg m^2)	5.0864×10^{-6}, 4.221×10^{-4}
J_{p6}, J_{d6} (kg m^2)	4.7578×10^{-4}, 2.6207×10^{-4}
J_{p7}, J_{d7} (kg m^2)	1.3359×10^{-6}, 9.6351×10^{-5}
J_{p8}, J_{d8} (kg m^2)	3.2499×10^{-6}, 8.3493×10^{-6}
J_{p9}, J_{d9} (kg m^2)	4.5272×10^{-6}, 3.35×10^{-6}
l_f (mm)	21

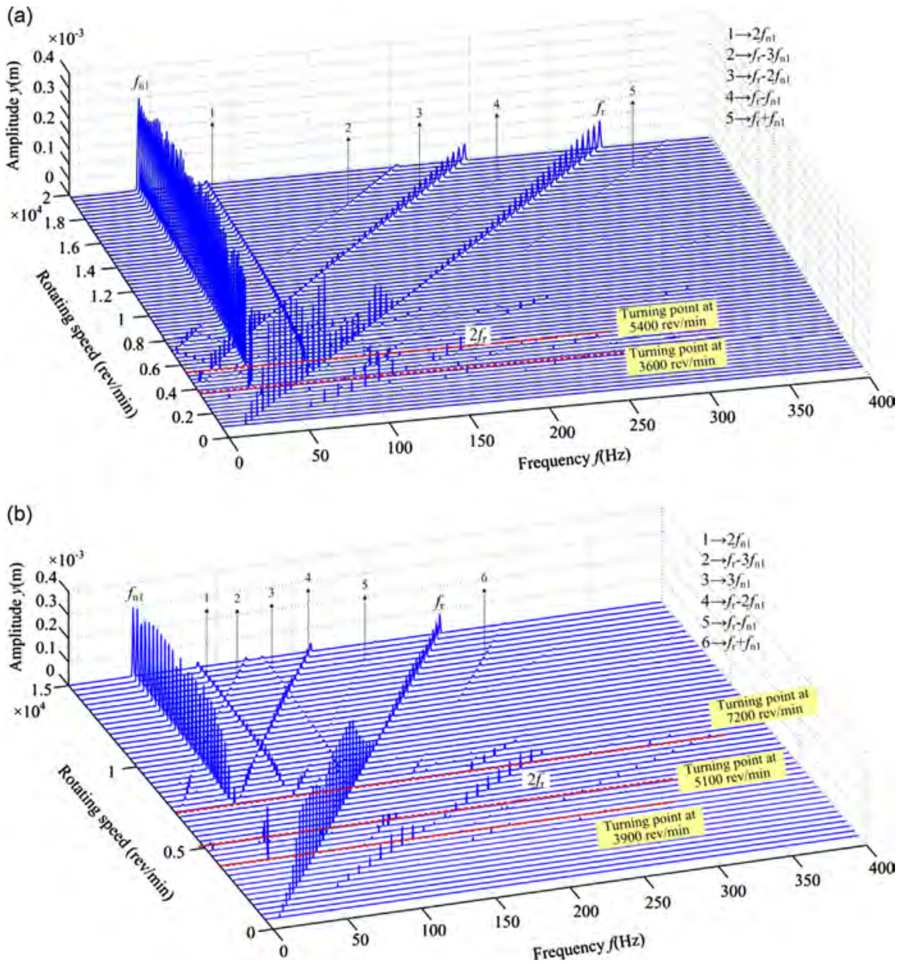

Fig. 25. Spectrum cascades in y direction under the first loading conditions: (a) rotor-bearing system and (b) rotor-bearing-seal system.

frequency is about 42 Hz, which remains close to the first natural frequency of the rotor (44 Hz), moreover, the amplitudes of oil whip are much higher than those of synchronous vibrations.

However, for the rotor-bearing-seal system, the first mode whirl appears in the range of $\omega\in[3900,5100]$ rev/min, and is replaced by synchronous vibration in the range of $\omega\in[5100,7200]$ rev/min, and then appears again when $\omega > 7200$ rev/min.

Based on the analyses above, it is clear that ranges of instability region decrease considering the effect of the seal; the first mode whip frequency and its amplitude show little change.

(2) Under the second loading condition, for the rotor-bearing system, the first mode whirl appears in the range of $\omega\in[3600,5700]$ rev/min, is replaced by synchronous vibration in the range of $\omega\in[5700,12,000]$ rev/min and occurs again when $\omega > 12,000$ rev/min and the corresponding whip frequency is about 43 Hz and are less than those of synchronous vibrations. The second mode whip appears and the amplitudes of the first mode whip decreases sharply when $\omega > 17,100$ rev/min, which shows the self-vibration energy is transferred from the first mode whip to the second mode whip. Moreover, the second whip frequency is about 145 Hz, which remains constant and is close to the second natural frequency (147.5 Hz).

However, for the rotor-bearing-seal system, the first mode whirl appears in the range of $\omega\in[3900,5400]$ rev/min and is replaced by synchronous vibration in the range of $\omega\in[5400,81,000]$ rev/min. Quasi-periodic motion (regular combination frequency components about f_r appear, such as low frequency components 54 Hz and 81 Hz at $f_r=135$ Hz, 71.94 Hz and 78.06 Hz at $f_r=150$ Hz, respectively) occurs in the range of $\omega\in[8100,96,000]$ rev/min and is replaced by synchronous vibration in the range of $\omega\in[9600,12,900]$ rev/min. The first mode whip occurs again when $\omega > 12,900$ rev/min and the second mode whip appear when $\omega > 17,100$ rev/min.

Compared with the features without considering the effect of the seal (see Fig. 26a), it is shown that the first instability region range for the first mode whirl decreases, moreover, the second instability threshold for the first mode whip increases

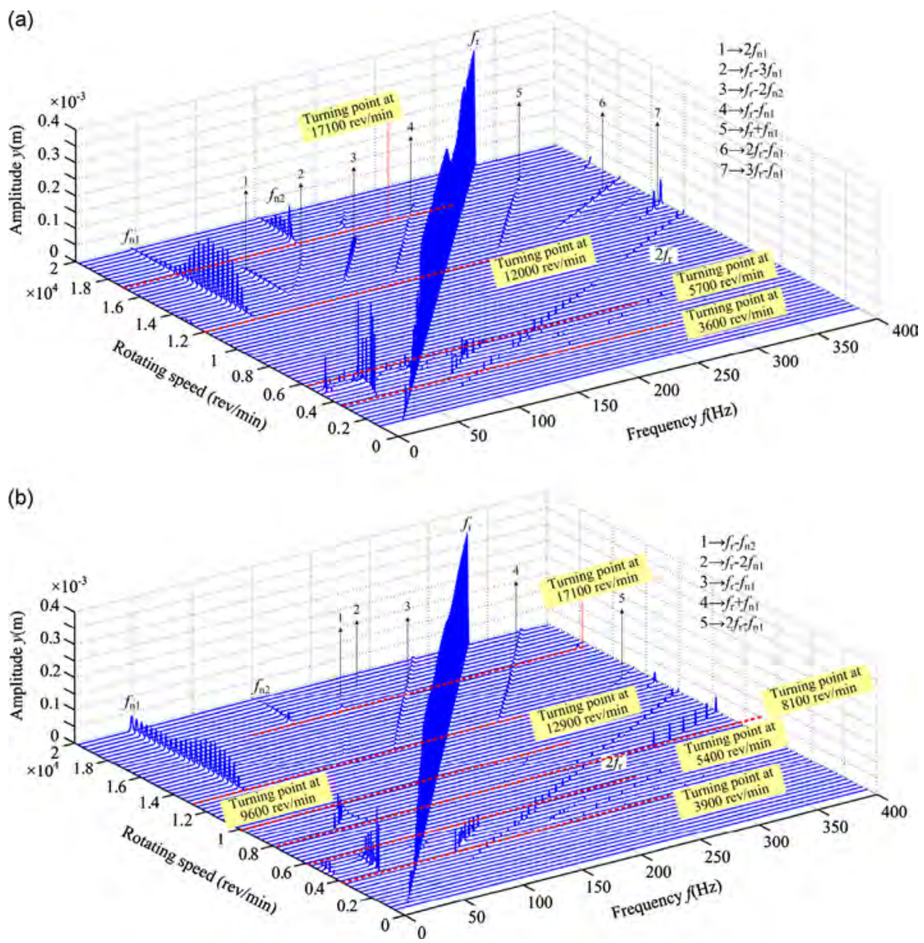

Fig. 26. Spectrum cascades in y direction under the second conditions: (a) rotor-bearing system and (b) rotor-bearing-seal system.

slightly and the threshold for the second mode whip remain unchanged considering the influence of the seal. It is worth noting that quasi-periodic motion (see Figs. 16a and 26b) will occurs at some rotating speeds between the first and second critical speeds in the rotor-bearing-seal system, however, does not appears in the rotor-bearing system. The nonlinear seal force should be primarily responsible for the appearance of quasi-periodic motion.

5. Conclusions

In this paper, the effects of the rotating speeds and the eccentrics of two discs on oil-film instability in a rotor-bearing-seal system under two loading conditions are investigated. A nonlinear oil-film force model based on short bearing assumption and Muszynska seal force model are adopted. The first and second mode instability laws are not only compared by including and excluding the seal effect in a rotor system with single-diameter shaft and two same discs and the instability laws are but also verified in a rotor system with multi-diameter shaft and two different discs. Some conclusions drawn from the study can be summarized as follows:

(1) For the rotor system with single-diameter shaft and two same discs under the first loading condition, the first mode instability threshold increases from 4800 rev/min (excluding the seal effect) to 6700 rev/min (including the seal effect). With the increasing eccentricity r of the disc, the whip amplitudes of the system excluding the seal effect are stable, however the first mode whip disappears at some r when the nonlinear seal force is considered. On the whole, the vibration intensity excluding the seal effect is greater than that including the seal effect, and the first mode whip frequency of the former is less than that of the latter. Namely, the seal force can restrain the occurrence of the first mode whip to some extent.

For the rotor system under the first loading condition, attached with multi-diameter shaft and two different discs, instability region ranges decrease due to considering the effect of the seal. Moreover, the first mode whip frequency and its amplitude show little change.

(2) For the rotor system with single-diameter shaft and two same discs under the second loading condition, the first mode instability threshold increases from 8700 rev/min (excluding the seal effect) to 13,500 rev/min (including the seal effect). For the former, the second mode instability appears at ω=12,000 rev/min, however, it appears at ω=14,130 rev/min for the latter. With the increase of eccentricity of the disc, the amplitude of the first mode whip at 16,000 rev/min decreases sharply and the amplitude of the second mode whip increases sharply for the former at r=0.16 mm, and the similar condition for the latter appears at r=0.225 mm. These features also show that the magnitude and phase of the unbalance could restrain the occurrence of the first and second mode whips.
For the rotor system with multi-diameter shaft and two different discs under the second loading condition, considering the nonlinear seal force, the first instability range for the first mode whirl decreases, the second instability threshold for the first mode whip increases slightly and the threshold for the second mode whip remain unchanged compared with those without considering seal effect.

(3) The oil-film instability threshold of the rotor system (considering the nonlinear seal force or not) under the second loading condition is higher than that under the first loading condition. Namely, the second loading condition can delay the first mode whips to some extent. Moreover, complicated combination frequency components about the rotating frequency f_r, the first mode instability frequency f_{n1} and the second mode instability frequency f_{n2} can be excited by the nonlinear oil-film force and seal force, and the second mode whip may appear under the second loading condition. Energy transfer phenomena occur between the first and second mode whips, that is to say, the amplitudes of two whip frequencies influence each other.

Conflict of interest

None.

Acknowledgments

We are grateful to the Natural Science Funds of China (NSFC, Grant no. 50805019), the Fundamental Research Funds for the Central Universities (Grant no. N100403008) and Program for New Century Excellent Talents in University (Grant no. NCET-11-0078) for providing financial support for this work.

References

[1] J.W. Lund, K.K. Thomsen, A calculation method and data for the dynamic coefficients of oil-lubricated journal bearings, *Proceedings of Topics in Fluid Film Bearing and Rotor Bearing System Design and Optimization, ASME Design Engineering Conference Publication*. April 1978, pp. 1–28.
[2] J.W. Lund, Stability and damped critical speeds of flexible rotor in fluid film bearings, *Journal of Engineering for Industry* 96 (1974) 509–517.
[3] G. Capone, Orbital motions of rigid symmetric rotor supported on journal bearings, *La Meccanica Italiana* 199 (1986) 37–46.
[4] G. Capone, Analytical description of fluid-dynamic force field in cylindrical journal bearing, *L'Energia Elettrica* 3 (1991) 105–110. (in Italian).
[5] W. Zhang, X. Xu, Modeling of nonlinear oil-film force acting on a journal with unsteady motion and nonlinear instability analysis under the model, *International Journal of Nonlinear Sciences and Numerical Simulation* 1 (2000) 179–186.
[6] G. Adiletta, A.R. Guido, C. Rossi, Nonlinear dynamics of a rigid unbalanced rotor in journal bearings, theoretical analysis, *Nonlinear Dynamics* 14 (1997) 57–87.
[7] J.P. Jing, G. Meng, Y. Sun, S.B. Xia, On the non-linear dynamic of a rotor-bearing system, *Journal of Sound and Vibration* 274 (2004) 1031–1044.
[8] J.P. Jing, G. Meng, Y. Sun, S.B. Xia, On the whipping of a rotor-bearing system by a continuum model, *Applied Mathematical Modelling* 29 (2005) 461–475.
[9] H.F. de Castro, K.L. Cavalca, R. Nordmann, Whirl and whip instabilities in rotor-bearing system considering a nonlinear force model, *Journal of Sound and Vibration* 317 (2008) 273–293.
[10] Q. Ding, A.Y.T. Leung, Numerical and experimental investigations on flexible multi-bearing rotor dynamics, *Journal of Vibration and Acoustics* 127 (2005) 408–415.
[11] Q. Ding, A.Y.T. Leung, Non-stationary processes of rotor/bearing system in bifurcations, *Journal of Sound and Vibration* 268 (2003) 33–48.
[12] Q. Ding, K.P. Zhang, Order reduction and nonlinear behaviors of a continuous rotor system, *Nonlinear Dynamics* 67 (2012) 251–262.
[13] W.M. Zhang, J.B. Zhou, G. Meng, Performance and stability analysis of gas-lubricated journal bearings in MEMS, *Tribology International* 44 (2011) 887–897.
[14] J.S. Alford, Protecting turbomachinery from self-excited rotor whirl, *ASME Journal of Engineering for Power* 87 (1965) 333–343.
[15] D.W. Childs, Dynamic analysis of turbulent annular seals based on Hirs' lubrication equation, *Journal of Lubrication Technology* 105 (1983) 429–436.
[16] A. Muszynska, *Rotordynamics*, CRC Taylor & Francis Group, New York, 2005.
[17] A. Muszynska, D.E. Bently, Frequency-swept rotating input perturbation techniques and identification of the fluid force models in rotor/bearing/seal systems and fluid handling machines, *Journal of Sound and Vibration* 143 (1990) 103–124.
[18] Z.G. Li, Y.S. Chen, Research on 1:2 subharmonic resonance and bifurcation of nonlinear rotor-seal system, *Applied Mathematics and Mechanics (English Edition)* 33 (2012) 499–510.
[19] S.T. Li, Q.Y. Xu, X.L Zhang, Nonlinear dynamic behaviors of a rotor-labyrinth seal system, *Nonlinear Dynamics* 47 (2007) 321–329.
[20] J. Hua, S. Swaddiwudhipong, Z.S. Liu, Q.Y. Xu, Numerical analysis of nonlinear rotor-seal system, *Journal of Sound and Vibration* 283 (2005) 525–542.
[21] Q. Ding, J.E. Cooper, A.Y.T. Leung, Hopf bifurcation analysis of a rotor/seal system, *Journal of Sound and Vibration* 252 (2002) 817–833.
[22] W.Z. Wang, Y.Z. Liu, G. Meng, P.N. Jiang, Nonlinear analysis of orbital motion of a rotor subject to leakage air flow through an interlocking seal, *Journal of Fluids and Structures* 25 (2009) 751–765.
[23] M. Cheng, G. Meng, J.P. Jing, Nonlinear dynamics of a rotor-bearing-seal system, *Archive of Applied Mechanics* 76 (2006) 215–227.
[24] M. Cheng, G. Meng, J.P. Jing, Numerical and experimental study of a rotor-bearing-seal system, *Mechanism and Machine Theory* 42 (2007) 1043–1057.
[25] X.Y Shen, J.H. Jia, M. Zhao, J.P. Jing, Experimental and numerical analysis of nonlinear dynamics of rotor-bearing-seal system, *Nonlinear Dynamics* 53 (2008) 31–44.

[26] X.Y Shen, M. Zhao, Effect of the seal force on nonlinear dynamics and stability of the rotor-bearing-seal system, *Journal of Vibration and Control* 15 (2009) 197–217.
[27] W. Li, D.R. Sheng, J.H. Chen, J.H. Chen, Y.Q. Che, Nonlinear dynamic analysis of a rotor/bearing/seal system, *Journal of Zhejiang University Science A (Applied Physics & Engineering)* 12 (2011) 46–55.
[28] W. Li, Y. Yang, D.R. Sheng, J.H. Chen, A novel nonlinear model of rotor/bearing/seal system and numerical analysis, *Mechanism and Machine Theory* 46 (2011) 618–631.
[29] Y.F. Wang, X.Y. Wang, Nonlinear vibration analysis for a Jeffcott rotor with seal and air-film bearing excitations, *Mathematical Problems in Engineering* (2010) 1–14. Article 657361.
[30] A. EI-Shafei, S.H. Tawfick, M.S. Raafat, G.M. Aziz, Some experiments on oil whirl and oil whip, *Journal of Engineering for Gas Turbines and Power* 129 (2007) 144–153.
[31] M. Friswell, J. Penny, S. Garvey, A. Lees, *Dynamics of Rotating Machines*, Cambridge University Press477–481.
[32] A. Muszynska, Stability of whirl and whip in rotor/bearing systems, *Journal of Sound and Vibration* 127 (1988) 49–64.
[33] API 617, *Axial and Centrifugal Compressors and Turboexpanders for Petroleum*, Chemical and Gas Industry Services, American Petroleum Institute, Washington, DC, 2002.